Available online at www.sciencedirect.com
ScienceDirect
Journal of Volcanology and Geothermal Research 158 (2006) 380–400
Journal of volcanology and geothermal research
www.elsevier.com/locate/jvolgeores

Clay minerals related to the hydrothermal activity of the Bouillante geothermal field (Guadeloupe)

A. Mas [a], D. Guisseau [a], P. Patrier Mas [a,*], D. Beaufort [a], A. Genter [b], B. Sanjuan [b], J.P. Girard [b]

[a] *Université de Poitiers, laboratoire HYDRASA, UMR 6532 du CNRS, 40 avenue du recteur Pineau, 86022 Poitiers cedex, France*
[b] *BRGM, 3 avenue Claude Guillemin, 45060 Orléans cedex 2, France*

Received 17 March 2006; received in revised form 27 June 2006; accepted 5 July 2006
Available online 22 September 2006

Abstract

The geothermal field of Bouillante (Guadeloupe, FWI) is a high-enthalpy hydrothermal system emplaced in submarine volcanoclastic formations (hyaloclastites, scarce lava flows) and subaerial formations (andesitic lava flows, pyroclastites, lahars) which belong to the Lesser Antilles arc. Three directional wells were drilled in 2001 to optimize the productivity of the geothermal field up to 15 MWe and to investigate the vertical distribution of clay alteration from the surface area down to a depth of 1000 m where temperatures exceed 250 °C. Special attention has been paid to the "clay signature" of the fractured zones which channel the present geothermal fluids.

Three successive zones, dominated, respectively by dioctahedral smectite, illite and chlorite were identified at increasing depths. Alteration petrography indicates that these mineralogical clay zones result from the spatial superimposition of at least two successive alteration stages.

The first one, assimilated to a propylitic alteration stage, affected all parts of the system and consisted of crystallization of trioctahedral phyllosilicates (chlorite or corrensite), Ca-silicates (heulandite-clinoptilolite, prehnite, pumpelleyite, wairakite and epidote), quartz and minor calcite in replacement of most of the primary minerals of the intersected volcanic or volcanoclastic formations. The later stage of alteration is related to the circulation of the present geothermal fluids and is assimilated to argillic or phyllic alteration. It consists of a more or less intense argillization which results from the crystallization of aluminous dioctahedral clay phases (smectite, illite±I–S mixed layers, and accessory kaolinite) associated with quartz, calcite, hematite or pyrite. The permeable zones which channel most of the present geothermal fluids are fracture controlled and do not contain specific clay parageneses. However the illite±I–S mixed layers minerals differ from those of the surroundings by specific properties including both crystal structure and texture. These specific properties (decrease in the expandable component of the illitic material, increase of the illite crystallinity) can be controlled by the nucleation/growth rates operating in zones of active flow regime. Being mainly a product of the earlier propylitic alteration stage, chlorites are much less informative on the fracture controlled permeable levels. However, the compositional variations of chlorites recorded within the shallower fractured zone suggest a significant change in fO_2 conditions related to early circulation of fluids along the major near west striking normal faults (Plateau fault).

Keywords: chemical composition; clay minerals distribution; microstructural and textural properties; high enthalpy geothermal field; Bouillante; geothermal fluid; thermal springs; Guadeloupe

* Corresponding author.
E-mail address: patricia.patrier@esip.univ-poitiers.fr (P. Patrier Mas).

0377-0273/$ - see front matter © 2006 Elsevier B.V. All rights reserved.
doi:10.1016/j.jvolgeores.2006.07.010

1. Introduction

Clay minerals are widespread alteration products in most of the active and fossil geothermal systems and, during the last thirty five years, the availability of these minerals which record in their crystal properties the hydrothermal history of the geothermal systems has been intensely investigated. Many studies have considered both the sequential distribution from smectites to non-expandable di- or trioctahedral phyllosilicates and the chemical variations of the non-expandable clay phases (*i.e.*, chlorite and/or illite) as a function of the past or present thermal conditions (McDowell and Elders, 1980; Inoue and Utada, 1983; Cathelineau and Nieva, 1985; Horton, 1985; Kranidiotis and MacLean, 1987; Harvey and Browne, 1991; Jowett, 1991; Patrier et al., 1996; Simmons and Browne, 1998; Ji and Browne, 2000 among many others). However, several authors have pointed out that the properties of clay minerals are not only affected by temperature but also by several factors such as rock and fluid chemistry, time, fluid/rock (*F*/*R*) ratio, the nature of the precursor material or the mechanism of crystal growth (Roberson and Lahann, 1981; Lonker et al., 1990; Beaufort et al., 1992; De Caritat et al., 1993; Inoue and Kitagawa, 1994; Chrisditis, 1995; Essene and Peacor, 1995; Beaufort et al., 1996; Martinez-Serrano and Dubois, 1998 among others).

The above factors influenced the crystal parameters of clays: structure (coherent domain size in the c-direction, polytypism, mixed-layering), composition (cation site occupancy) and texture (particle size, morphology) as did temperature. Consequently, the conditions at which these minerals crystallized in the active geothermal fields would be more properly approached by an integrated study of all the crystal parameters of clay minerals at the field scale.

The present study focuses on the clay minerals within the geothermal system of Bouillante (Guadeloupe, FWI), a high enthalpy geothermal system (with fluids at 242 °C produced at a 350 m depth) in which three additional wells were drilled in 2001. Clay minerals were extracted from cuttings and were characterized by a set of techniques including X-ray diffraction, scanning electron microscopy and chemical microanalysis. This study offers the opportunity to improve the knowledge of the geology of the geothermal reservoir in this field, and more particularly to elucidate how the structure, the chemistry and the texture of the clay minerals vary spatially as a function of combined factors measured or approached during the well logging operations (temperature, rock and fluid composition, fluid/rock ratio). Special attention has been paid to the mineralogical signature of clay minerals from the fractured zones which produce the present geothermal fluids.

2. Geological setting

The geothermal field of Bouillante is located on the western coast of the Basse-Terre island (Guadeloupe), which belongs to the active volcanic island arc of the Lesser Antilles (Fig. 1). The development of the Bouillante geothermal system started in 1970, when four exploration wells (BO1, BO2, BO3 and BO4) were drilled in an area characterized by hydrothermal surface manifestations such as hot springs, mud pools, steaming ground and fumaroles. Among the four exploration wells, only BO2 was revealed as a good productive well and was producing about 150 t/h of geothermal fluid (whose 30 t/h of steam) between 1986 and 1992 and between 1996 and 2002. In 2001, three directional wells (BO5, BO6 and BO7) were drilled in the BO4 platform (elevation ~ 90 m). Among these wells, only BO5 and BO6 were productive with the well BO4 thermally stimulated in 1998 (Correia et al., 2000). They are presently exploited by a new geothermal power plant which enhances the present productivity of the geothermal field of Bouillante up to 15 MWe.

The geothermal activity of the area could be related to a fissural volcanic activity which is supposed to be related to a major regional tectonic structure oriented NNW–SSE (the Basse-Terre–Montserrat fault system) (Traineau et al., 1997). The recent volcanic activity is expressed by the "Bouillante Volcanic Chain" (−0.8–0.6 Ma) which generated several volcanic centers (Traineau et al., 1997). The geothermal area of Bouillante is located at a convergence point between the NNW–SSE-striking faults system, mainly recognized offshore, and ~ east–west-striking normal faults observed on the island, which display a geometry similar to that observed farther east between Grande Terre and Marie Galante (Marie Galante graben) (Feuillet et al., 2002).

On the island, the tectonic fracturation, mainly organized into a major set striking N100–120° (Traineau et al., 1997) with vertical dip, consists of normal faults and fractures sealed by secondary minerals. The hydrothermal veins (a few millimeters to centimeter wide) are restricted to the Bouillante area. They underline the close association between fracturation and circulation of hydrothermal fluid and are interpreted as the result of the discharge of high temperature fluids. The hydrothermal parageneses are composed of silica (quartz or other forms of silica), dioctahedral smectites, calcite, zeolites (clinoptilolite, heulandite, stilbite, mordenite)

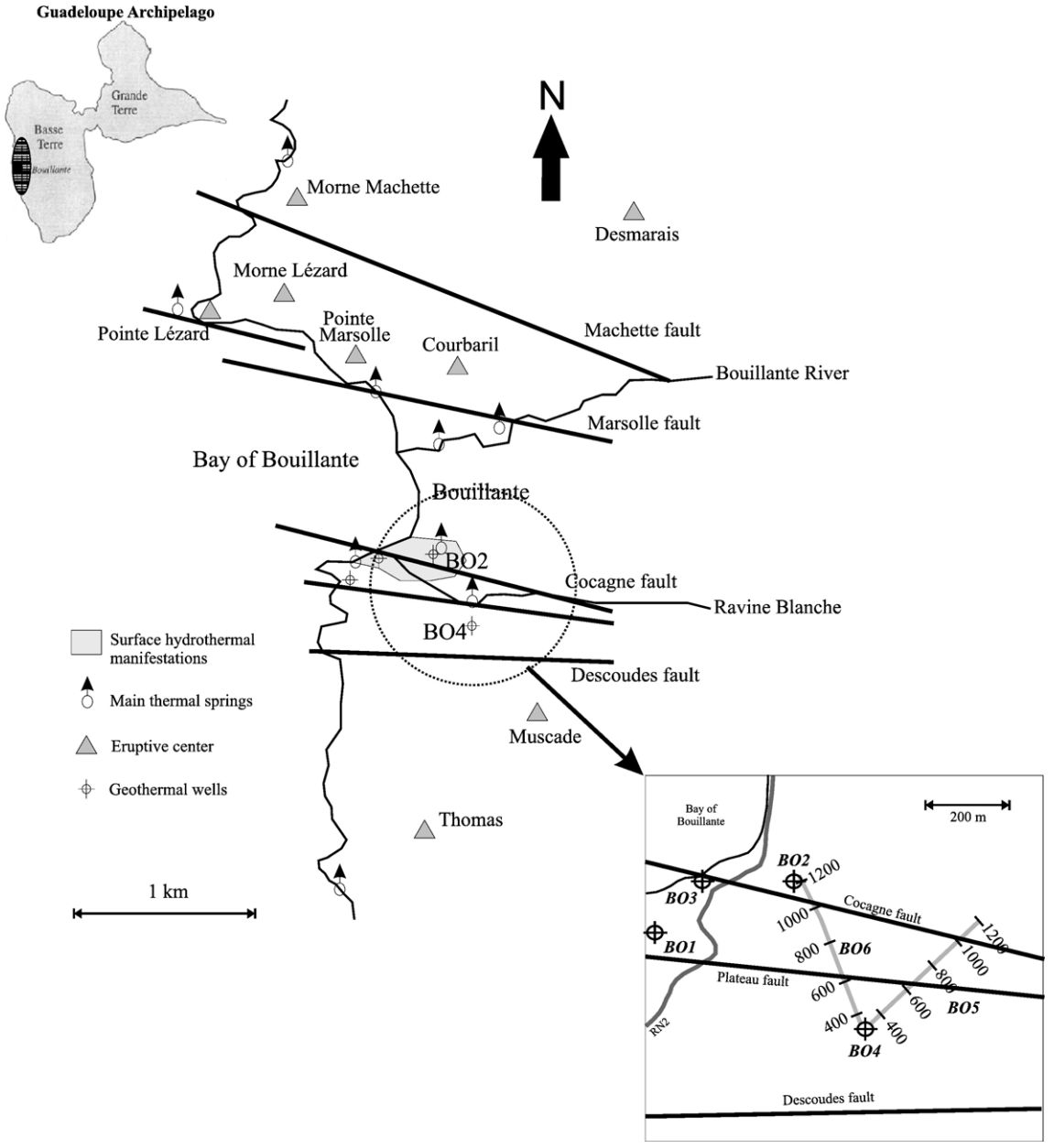

Fig. 1. Location of the studied area in Guadeloupe island and schematic map of the Bouillante Bay showing the location of the ancient and new wells, and the main surface hydrothermal manifestations. The bold lines represent the main tectonic faults identified by Traineau et al. (1997).

and accessory kaolinite and gypsum. They are mostly located in the southern part of the Bouillante Bay, in close association with the geothermal surface manifestations, and along the northern coastline of the Bouillante bay, up to Pointe Lézard, in absence of any active hydrothermal manifestations (Patrier et al., 2003).

The substratum of the field consists of intercalation of submarine, volcanoclastic formations (hyaloclastites, scarce lava flows) and subaerial formations (andesitic lava flows, pyroclastites, lahars) mainly attributed to the activity of the axial chain (−1.5–0.6 Ma).

Most chemical and physical characteristics of the collected geothermal fluids are quite similar between all the different productive wells suggesting a common origin for the deep geothermal fluid (Traineau et al., 1997; Sanjuan et al., 2001). Chemical and isotopic compositions of some thermal springs and the geothermal fluid discharged from the wells BO2, BO4, BO5

and BO6 in the Bouillante area are listed in Table 1. The deep geothermal fluid consists of high temperature NaCl brine with TDS around 20 g/l and a pH of 5.3±0.3 resulting from a mixture between 58% seawater and 42% fresh water, which reacted with volcanic rocks and reached equilibrium at 250–260 °C in the reservoir with a mineralogical assemblage including quartz, albite, K-feldspar, calcite, disordered dolomite, anhydrite, illite, smectites, laumontite, heulandite and wairakite (according to saturation calculations using the EQ3NR geochemical modeling code). Compared to a seawater diluted by 42% of fresh water, the geothermal brine is depleted in Mg, SO_4, Na and enriched in K, Ca, Si, B, NH_4, H_2S, Li, Sr, Ba, Mn, Cs, Rb, As and trace metal ions. Its $^{87}Sr/^{86}Sr$ ratio is close to that measured in the volcanic rocks such as andesites or basalts. The δ^7Li and $\delta^{11}B$ signatures are far from the values analyzed in the seawater (30 and 40‰, respectively) and confirm the importance of the processes of fluid–rock interaction. The results obtained during inter-well tracer tests

Table 1
Chemical and isotopic compositions of some thermal springs and the geothermal fluid discharged from the wells BO2, BO4, BO5 and BO6 in the Bouillante area

	Riv. Bouillante amont	Lise	Bain du curé	Marsolle	Tuyau	Thomas	Submarine spring	BOBS drill-hole	Reconstructed composition for the fluid discharged from the geothermal wells
T (°C)	30	36	39	44	61	54	94	94	250–260
pH	7.13	7.26	7.40	7.18	6.29	6.78	6.27	6.84	5.30
TDS (g/l)	0.32	0.30	0.32	0.80	2.0	12	27	27	20
Na (mg/l)	30	41	41	171	435	3200	7500	7210	5100
K (mg/l)	9.8	3.9	3.9	16	43	204	619	750	750
Ca (mg/l)	20	12	20	44	212	843	1358	2340	1800
Mg (mg/l)	9.7	6.1	3.5	13	11	166	533	5.8	2.0
Cl (mg/l)	32	27	29	277	929	7105	15,545	16,400	12,000
HCO_3 (mg/l)	137	125	130	167	156	69	321	3.7	50
SO_4 (mg/l)	3.8	4.8	6.7	29	94	326	1149	83	17
SiO_2 (mg/l)	75	77	82	87	127	142	201	147	500
H_2S (mg/l)	*n.a.*	*n.a.*	*n.a.*	*n.a.*	*n.a.*	*n.a.*	*n.a.*	*n.a.*	10
Br (mg/l)	0.12	0.12	0.11	0.93	3.6	24	53	63	42
B (mg/l)	0.041	0.057	0.055	0.22	0.50	5.0	10	12.5	12.5
F (mg/l)	*n.a*	*n.a.*	*n.a.*	0.2	<0.5	0.3	1.0	<1	0.9
NH_4 (mg/l)	*n.a.*	*n.a.*	*n.a.*	<0.1	7.9	1.1	0.4	2.2	1.7
Sr (mg/l)	0.084	0.058	0.082	0.30	1.62	7.8	14.7	25.4	16
Mn (mg/l)	0.0012	0.0053	0.00028	0.00018	1.0	0.66	3.6	4.0	4.8
Ba (mg/l)	0.0037	0.0041	0.0073	0.0078	0.10	0.51	0.27	4.7	6.5
Fe (mg/l)	<0.02	<0.02	<0.02	<0.02	<0.02	<0.02	0.34	<0.02	3.2
Li (mg/l)	0.0023	0.0018	0.0036	0.0458	0.13	1.9	3.0	5.1	5.0
Rb (mg/l)	0.0074	0.0088	0.0138	0.0319	0.14	0.37	1.0	2.3	2.2
Cs (μg/l)	0.10	0.10	0.19	2.8	26	66	105	310	260
As (μg/l)	0.5	1.7	1.5	3.5	12	176	146	490	450
Al (μg/l)	<10	<10	<10	<10	<10	<30	60	<100	60
Cu (mg/l)	<0.005	<0.005	<0.005	<0.005	<0.005	0.012	0.020	0.014	15
Ni (mg/l)	<0.005	<0.005	<0.005	<0.005	<0.005	0.024	0.037	0.017	2.0
Zn (μg/l)	<5	<5	<5	<5	<5	16	16	49	650
Co (μg/l)	<5	<5	<5	<5	<5	5.0	11	14	13
Cr (μg/l)	<5	<5	<5	<5	<5	<5	8	<10	15
Pb (μg/l)	<5	<5	<5	<5	<5	*n.a.*	*n.a.*	<10	4.0
dD (‰)	−8.3	−8.2	−8.5	−8.1	−9.5	−6.1	2.8	3.8	−1.2
$d^{18}O$ (‰)	−2.7	−2.6	−2.8	−2.6	−2.6	−1.4	−0.3	−0.1	−1.1
$d^{34}S$ (SO_4)(‰)	*n.a.*	*n.a.*	9.6	*n.a.*	*n.a.*	18.6	19.6	19.3	18.9
$d^{18}O$ (SO_4)(‰)	*n.a.*	*n.a.*	8.7	*n.a.*	*n.a.*	*n.a.*	8.8	*n.a.*	5.6
$^{87}Sr/^{87}Sr$	*n.a.*	*n.a.*	0.704066	0.705170	0.704726	0.705208	0.706171	*n.a.*	0.704960
$d^{11}B$ (‰)	*n.a.*	*n.a.*	*n.a.*	22.5	*n.a.*	*n.a.*	*n.a.*	15.7	16.3
$d^{11}Li$ (‰)	*n.a.*	*n.a.*	14.5	5.8	*n.a.*	5.4	4.8	4.2	4.4
$d^{13}C$ (‰)	*n.a.*	*n.a.*	*n.a.*	*n.a.*	*n.a.*	*n.a.*	*n.a.*	*n.a.*	−3.9

n.a.: not analyzed.

conducted in 1998 (Correia et al., 2000) and the $\delta^{18}O$ signature indicate the absence of any ^{18}O enrichment due to interaction with silicate or carbonate minerals. This argues for the existence of a relatively large interconnected reservoir volume (>30 millions m^3) and a high *F*/*R* ratio. In the present exploitation conditions, the temperature and pressure of fluid separation are 167 °C and 7.4 bar, respectively. The steam condensate collected after the phase separator has a low salinity (TDS < 80 mg/l), a relatively high concentration of dissolved H_2S (35–45 mg/l) and is enriched in NH_4 (4.5–5.0 mg/l). Its pH values range from 4.1 to 4.5 whereas neutral pH is found for the separated water. The chemical and isotopic composition reconstructed for the incondensable gases associated with the fluid discharged from the wells (about 4 kg of gases for 1 t of produced steam and 4 t of discharged geothermal water) is given in Table 2. CO_2 is the predominant gas and the $\delta^{13}C$ signature suggests a mixed magmatic and marine (or sedimentary) origin for CO_2. The N_2/Ar ratio indicates a dominant atmospheric origin for these gases. Both the He/Ar and $^3He/^4He$ ratios, intermediate between the atmospheric ones and those measured at the summit of the Soufrière volcano in Guadeloupe, indicate that a significant amount of He has a magmatic origin. The concordant temperatures estimated using gas geothermometers (230–250 °C) suggest that most of the gases (CO_2, CH_4, H_2, H_2S, He, and Ar) are close to equilibrium at the reservoir conditions.

Table 2
Chemical and isotopic composition reconstructed for the incondensable gases related to the geothermal fluid discharged from the wells BO2, BO4, BO5 and BO6

	Reconstructed composition for the incondensable gases discharged from the wells
GSR (mass %)	0.4
CO_2 (vol.%)	93
N_2 (vol.%)	3.5
H_2S (vol.%)	2.7
CH_4 (vol.%)	0.4
H_2 (vol.%)	0.4
Ar (vol.%)	0.04
He (vol.%)	0.0035
C_2H_6 (vol.%)	0.004
C_3H_8 (vol.%)	0.0005
O_2 (vol.%)	0
N_2/Ar (vol.)	88
He/Ar (vol.)	0.09
$\delta^{13}C$ (‰)	−2.6
$(^3He/^4He)/(^3He/^4He)_{atmospheric}$	4.6

GSR: Gas Steam Ratio. In the present exploitation conditions, for 1 t of produced steam and 4 t of produced separated water (5 t of geothermal fluid), about 4 kg of CO_2 are discharged.
N_2/Ar atmospheric ratio is close to 84.
He/Ar ratios higher than 0.1 indicate a magmatic origin.

Thermal waters (up to 96 °C) have been identified all around the bay of Bouillante. Two groups have been distinguished (Traineau et al., 1997; Brombach et al., 2000): (1) superficial Na–HCO_3 waters (salinity ≤ 1 g/l, pH = 7–8), of meteoric origin and heated through conductive heat transfer (thermal springs such as "Rivière Bouillante amont", "Lise" and "Bain du Curé" reported in Table 1); (2) NaCl waters of marine origin (mass Cl/Br ratio close to 290), with salinity up to 35 g/l, which resulted from mixtures of two or three water end-members (seawater, superficial water of meteoric origin and the deep geothermal fluid; the other springs reported in Table 1).

The rare fumaroles, located in steaming grounds near the geothermal power plant, were studied by BRGM in 1997 and 1999 (internal reports) and by Brombach et al. (2000). The analytical results of the incondensable gases indicate mixtures between deep gases associated with the geothermal fluid (dominated by the presence of CO_2) and air, at different proportions. The δD and $\delta^{18}O$ values analyzed in the vapor phase show that this latter can be either separated from the geothermal fluid after dilution with cold groundwater down to 100 °C, or produced through steam separation at about 100 °C from the undiluted geothermal fluid, followed by condensation or by an intermediate process (Brombach et al., 2000).

3. Well data and sampling

The sampling has been focused on well BO6. This well was drilled along a vertical axis from the surface to 300 m depth, and takes a N34W direction after 300 m and up to 1248 m (drilling depth) (Fig. 1). It should be noted that the depth values indicated in this paper refer to the drilling depths. Only a few additional shallow samples have been collected in the well BO5 drilled just a few meters from BO6. The bottom of the well BO6 is located exactly 700 m under the reservoir already exploited through the well BO2, right below the geothermal power plant. BO6 well intersects two normal faults: the Plateau fault and the Cocagne fault at drilling depths around 600 m and 1000 m, respectively (Fig. 1).

The preliminary geological data (lithology, measured downhole temperatures) were provided by CFG Services (Table 3).

From 0 to 474 m, the lithology consists of subaerial volcanic formations (lahars and tuffs alternating with

Table 3
Sampling carried out in BO5 and BO6 wells

Drilling depth (m)	NGF alt. (m)	Sampling
BO6 drill hole		
125	−40	Lava horizon: porphyric andesitic lava, more or less altered and argillized
135	−50	*Tuff/lahar*: brecciated formation with a fine texture, argillized
160	−75	Hydrothermalized fractured zone: very argillized tuff/lahar, locally silicified with abundant calcite
200	−110	Hydrothermalized fractured zone: formation of very argillized tuff with kaolinite, green clay, calcite, pyrite
246	−160	Lava horizon: subaphyric andesitic lava poorly altered
260	−169	Hydrothermalized fractured zone: very argillized lava with kaolinite, green clay, calcite, pyrite
310	−210	Lava horizon: aphyric to subaphyric andesitic lava poorly or not altered
345	−250	Tuff: silicified and chloritized formation with lava elements. Epidote appears near 350m
415	−319	Lava horizon: subaphyric andesitic lava poorly altered. Numerous fragments of secondary deposits of silica and carbonates. Low amount of epidote.
459	−360	Tuff: chloritized and silicified formation, epidote in low amount
494	−390	Hyaloclastic tuff: brecciated formation with fine texture. Very few lava fragments. Vesicles filled by silica and chlorite
520	***−410***	
540	***−426***	
556	***−440***	*Lava horizon*: subporphyric lava, more or less altered
574	***−455***	*Tuff*: coarse brecciated formation, with more or less oxidized lava fragments, abundant silica and chlorite
595	***−475***	*Hyaloclastic tuff*: fine to very fine texture, very few lava fragments. Vesicles mainly filled by silica and chlorite
610	−480	
620	−490	
640	−510	*Hyaloclastic tuff*: fine to very fine texture, very few lava fragments. Epidote discrete to abundant. Low amount of pyrite. Geodic quartz
650	−518	
660	−525	
705	−560	Hyaloclastic tuff: fine to very fine texture, silicified and chloritized, few lava fragments. Epidote present.
720	−574	
780	−630	Hyaloclastic tuff: fine to very fine texture, silicified and chloritized, with very few lava fragments. Epidote abundant
836	−665	
850	***−680***	
860	***−685***	
870	***−695***	*Lava horizon*: aphyric lava poorly altered
877	***−710***	*Hyaloclastic tuff*: fine to very fine texture, silicified and chloritized, with very few lava fragments. Epidote abundant
891	***−720***	*Hyaloclastic tuff*: fine to very fine texture, silicified and chloritized. Epidote abundant
900	***−725***	
910	***−730***	*Hyaloclastic tuff*: fine to very fine texture, silicified and argillized. Epidote abundant. Geodic quartz.
BO5 drill hole		
60	+25	Lahars and tuffs
100	−5	
125	−40	
130	−50	
155	−60	Argillized fractured zone
160	−75	Lahars and tuffs
185	−95	Argillized fractured zone
200	−110	Massive lava horizon: microlithic andesitic lava with plagioclase and pyroxene phenocrysts, presence of chlorite, silica, carbonates, anhydrite, pyrite as vein and vesicle infilling
250	−155	*Lahar/tuff*: formation of tuff and clayey lahar. Hydrothermal alteration with probable fractured zones, abundant white clay phases, silica, pyrite, chlorite. Anhydrite in low amount
260	−175	
300	−205	*Massive lava horizon*: aphyric to subaphyric, fresh to slightly altered, with disseminated fissures infilled by hydroxides, pyrite, or silica+carbonates+pyrite+chlorite assemblages
307	−210	

Lithology and field observations were provided by CFG services.
Zones of active flow regime zones are located between 500 and 595 m and from 850 m.

andesitic lava horizons). Hydrothermalized fractured zones have been encountered in the range of 154–161 m, 188–206 m, 226–236 m and 259–269 m. From 474 m to 1248 m, submarine volcanic formations consist of hyaloclastic tuffs, which alternate with rare andesitic lava horizons.

Circulation losses during drilling, or well tests, (between 500 and 590 m, and from 850 m) revealed high permeable zones. The first zone coincides with the permeable damage zone of the Plateau fault and the second one, which coincides with the top of the reservoir zone, corresponds to the damage zone of the Cocagne fault. Fluids were only recovered from these two levels and consist of the analyzed alkali chloride geothermal fluids.

The downhole temperatures measured in the range 100 to 910 m vary from 80 °C to 260 °C (Fig. 2).

Special attention was paid to the permeable and fractured levels during the sampling. Forty cutting samples were collected between 60 and 910 m (Table 3). Each of them is representative of a 3-m-thick lithological column. Important drilled mud losses during drilling prevented the recovery of cuttings in the lower part of the drill hole.

4. Analytical methods and sample preparations

Samples were ground in an automatic shatterbox. The powders were then dispersed in distilled water by

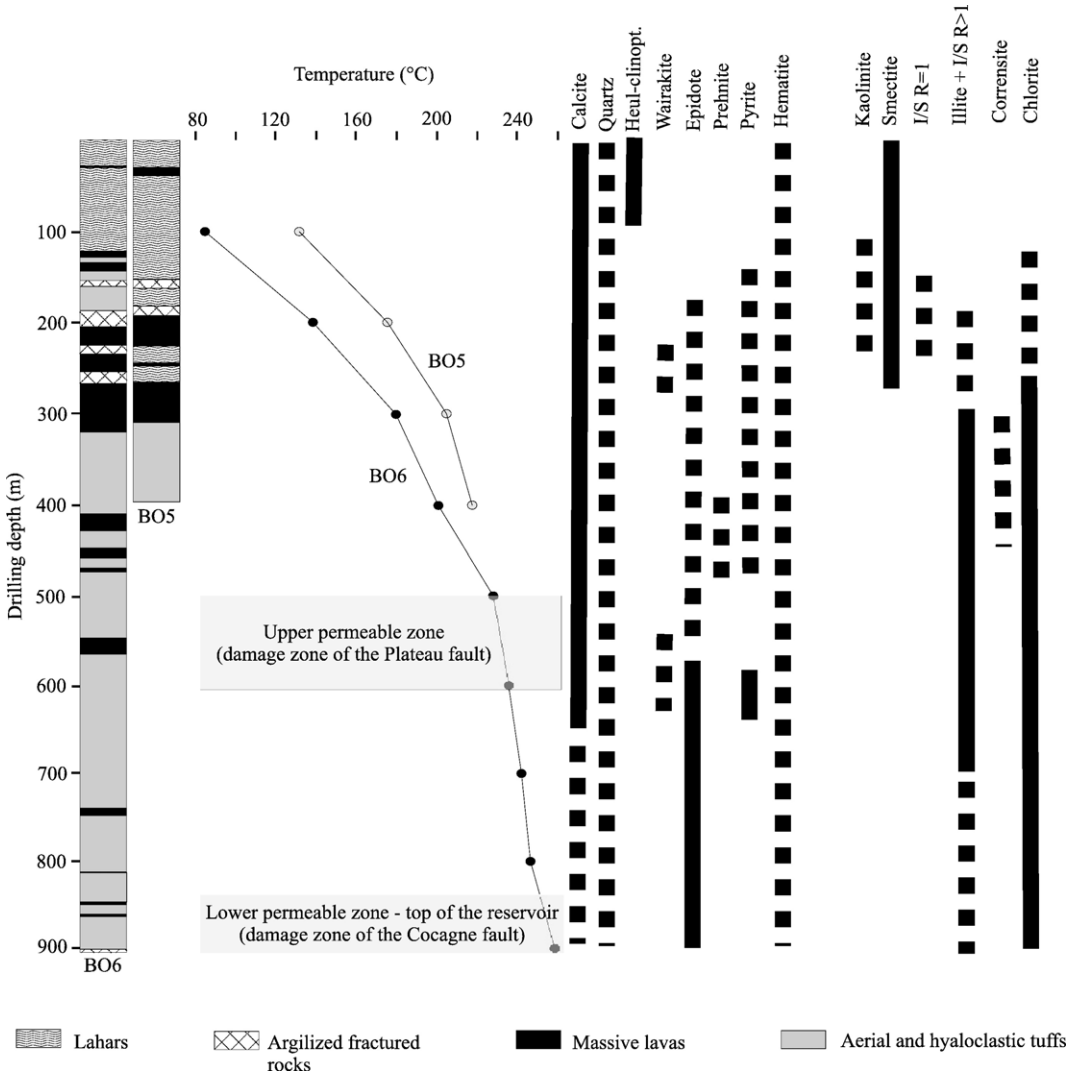

Fig. 2. Lithology and distribution of secondary minerals in BO6 and in the upper part of BO5 wells. The temperature profiles correspond to the present day temperatures. The two permeable levels associated with the damage zones of the Plateau and the Cocagne faults are shown (between 500 and 590 m and from 850 m, respectively).

ultrasonic vibrations to disintegrate the particles. Bulk rock chemical analyses were performed by BRGM on samples ground at 80 μm using the X-ray fluorescence method (Philips Panalytical PW2400, Li tetraborate used for sample melting). Relative analytical uncertainty is lower than 1 to 5%, depending on the analyzed species. Oriented mounts on glass slides were made with the infra 2 μm clay suspension, obtained by centrifugation (JOUAN GR422, rotor speed = 1000 r.p.m. during 2 mn 30 s). A finer fraction (<0.2 μm) was extracted by continuous ultracentrifugation (BECKMAN J22, rotor speed = 5000 r.p.m., flow rate = 150 ml/min). This recovered fraction was Ca-saturated ($CaCl_2$, 1 N), in order to minimize the hydration heterogeneity of smectite interlayers.

Comparison between diffraction patterns of the coarse-grained (less than 2 μm) and the fine-grained (less than 0.2 μm) fractions indicated that the latter gives more accurate information on the clay material, as already proved in previous studies (Patrier et al., 1996). These XRD patterns are very weakly affected by impurities of non-platy minerals such as quartz. Moreover, because the small particles are the most reactive parts of an altered rock, inherited minerals would be minimized in this fine clay fraction (Jennings and Thompson, 1986; Harvey and Browne, 1991).

X-ray diffraction (XRD) was performed on randomly oriented powders and oriented mounts of untreated and ethylene–glycol saturated samples. XRD was carried out on a Philips PW1729 diffractometer (CuKα radiation, 40 kV, 40 mA) monitored by a DACO MP numerical system (SOCABIM). The conditions of acquisition are presented in Table 4. XRD data acquisition and treatment were realized with the DIFFRAC AT software. Clay minerals were identified according to Brindley and Brown (1980). Identification of clay species was primarily based on the position of (00*l*) spacings after saturation with ethylene–glycol. The percentage of illite in the illite/smectite mixed layers was estimated by using the Newmod calculation program (Reynolds, 1985).

Chlorite and illite coherent scattering domain (CSD) sizes along the c* axis were estimated from the full width at half maximum intensity (FWHM) of the typical (00*l*) reflections at 7 Å and 10 Å, respectively, on ethylene–glycol saturated oriented preparations of the <2 μm and <0.2 μm fractions (Kubler, 1968). Although more advanced methods have been developed recently (Drits et al., 1997), this method still remains convenient for both illite and chlorite (Guggenheim et al., 2002). In the presence of expandable components, FWHM measurements of the clay minerals were performed on the appropriate elementary curves calculated from the mathematical deconvolutions of the (00*l*) reflections, using the DECOMPXR software (Lanson and Besson, 1992).

Chemical analyses of clay minerals were carried out on a Cameca SX50 electron microprobe equipped with wavelength dispersive spectrometers. The analytical conditions were the following: 4 nA, 15 kV, spot size of 4 μm, counting time of 10 s/element. Elements analyzed were Si, Al, Fe, Mg, Mn, Ti, Ca, Na and K. The system was calibrated with a variety of synthetic oxide and natural silicate standards ($MnTiO_3$, hematite, albite, orthoclase and diopside) and corrections were made with a ZAF program. The reproducibility of standard analyses was close to 1% except for Na, which was 1.5%.

The morphological observation of clay minerals was performed with a scanning electron microscope (SEM-JEOL 5600 LV). Observations were carried out on carbon coated rock slabs a few millimeters wide. Quantitative composition of clay minerals was done by a coupled EDS equipment (Si(Li) diode). Analytical conditions were as follows: accelerating voltage 15 kV, probe current 0.6–0.7 nA.

Table 4
Conditions of acquisition of X-ray diffraction data: angular domain, step increment and counting time per step

	Angular domain (°2θ, CuKα)	Step increment (°2θ, CuKα)	Counting time per step (s)
Clay powder (06,33)	60–64	0.020	10
Randomly oriented powder mount	2.5–65	0.025	3
Oriented mount	2.5–30	0.025 [a]	3 [a]

[a] Scanning speed used to measure the FWHM values.

5. Alteration petrography and vertical distribution of clay minerals

Even if lava flows are less altered than the permeable volcanoclastic formations, the lithological sequence intersected by BO6 bore hole displays a broad alteration zoning marked by changes in the nature of secondary phyllosilicates (Fig. 2), and by common superimposition of several alteration parageneses. The alteration products identified from XRD patterns (Figs. 3 and 4) are dominated by smectite at shallow depth (0–260 m, 70 to 160 °C), and by variable amounts of illitic minerals and chlorite at greater depth (260–920 m, 160–

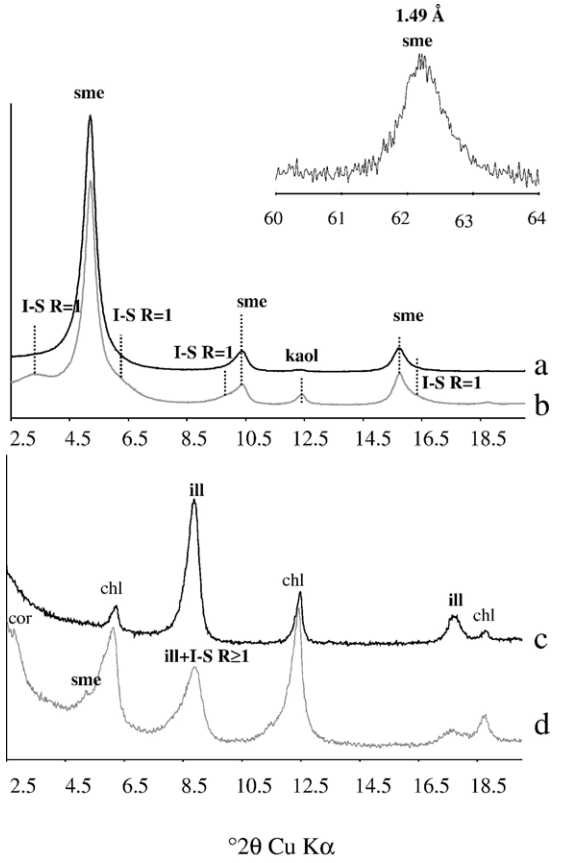

Fig. 3. X Ray diffractograms of the dioctahedral clay phases, as observed in BO6 well. sme: di-smectite; I–S $R=1$: regularly ordered illite/smectite mixed-layers; I–S $R\geq 1$: ordered illite/smectite mixed-layers with high illite content (>85%); ill: illite. Trioctahedral phases also identified: chl: chlorite, cor: corrensite. a: BO6, 125 m; b: BO6, 160 m; c: BO6, 574 m; d: BO6, 415 m. Ethylene–glycol saturated samples.

260 °C). The term illitic minerals will be used hereafter for clay-size mineral assemblage dominated by discrete illite but still containing a significant proportion of highly illitic (>90% illite) I–S mixed layers (Meunier et al., 2000).

5.1. The smectite zone

Within the upper part of the drill holes (0 to 260 m), most of the rock forming minerals (plagioclases and pyroxenes) have been strongly dissolved and replaced by a smectite+calcite±hematite assemblage. Smectite and calcite predominate (Fig. 5a) but they are commonly associated with mixtures of secondary minerals including variable but generally minor amounts of quartz, zeolites (heulandite–clinoptilolite), kaolinite, illite/smectite mixed layers, illite, chlorite, hematite or pyrite. Alteration petrography indicates that smectite and calcite are the newly formed mineral assemblage. This alteration stage obliterated the previously formed secondary silicate minerals whose mineralogy seems to be depth related: zeolites of the heulandite–clinoptilolite group (0–125 m, 80–100 °C), wairakite, minor pumpelleyite and epidote (from 246 m, for $T>150$ °C) and disseminated minerals of the chlorite group (corrensite, chlorite) which previously replaced primary pyroxenes and glass inclusions at depths below 125 m (Fig. 5b). Very low amounts of regularly ordered illite/smectite mixed-layers (I–S $R=1$) have been detected in XRD patterns of samples collected between 150 m and 250 m (110 °C $\leq T\leq$ 160 °C) (Fig. 3). However, due to the small size of the studied cuttings, the mutual relationships between the illite/smectite mixed layers and the discrete smectite were not clearly established enough to comment on their relative chronology. Kaolinite is restricted to hydrothermal deposition in microfractured levels. It occurs as vermicular booklets, partly replaced by folded thin films of smectite.

Several generations of calcite have been identified. Among them, blade shaped calcite crystals,

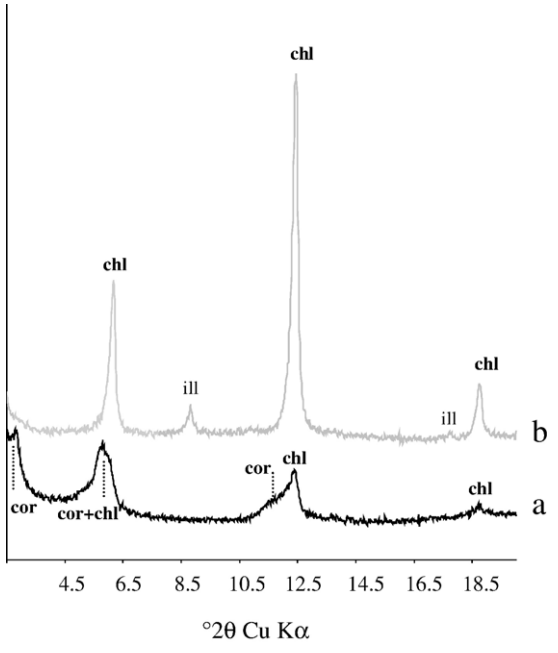

Fig. 4. X Ray diffractograms of the trioctahedral clay phases, as observed in the BO5 and BO6 wells. cor: corrensite, chl.: chlorite. Dioctahedral phases also identified: ill: illitic phases. a: BO5, 300 m; b: BO6, 850 m. Ethylene–glycol saturated samples.

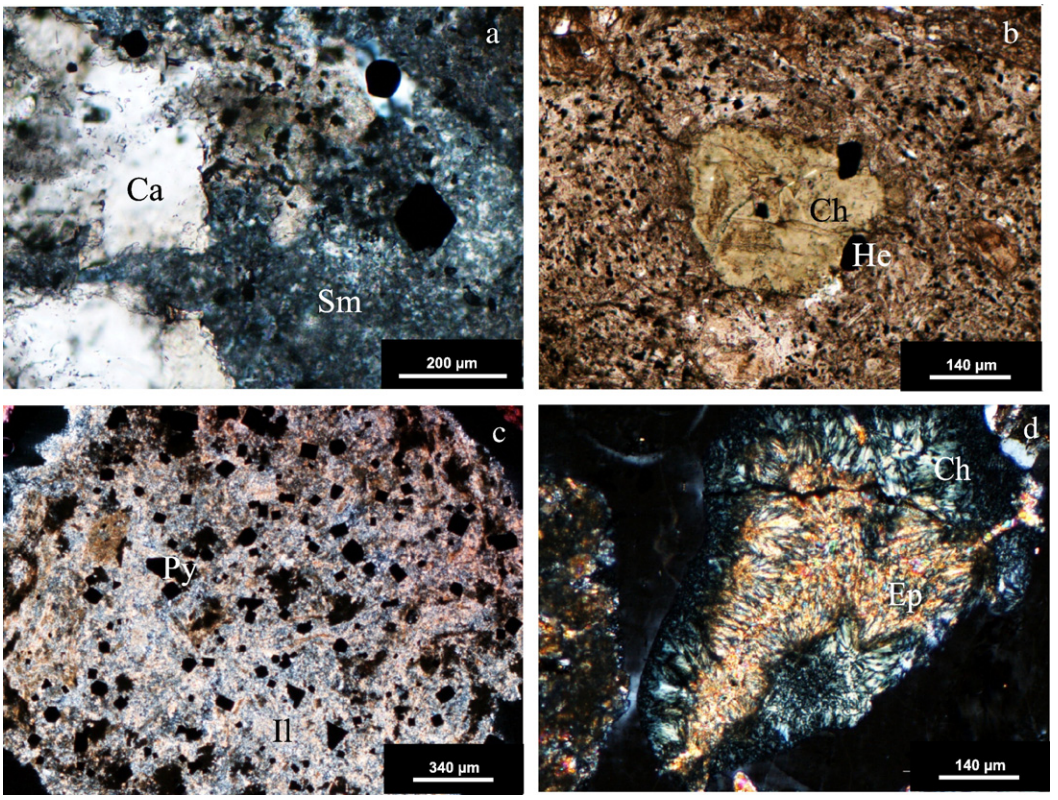

Fig. 5. (a) In the most surficial zone, the groundmass of the rock can be totally replaced by calcite "Ca" and by dioctahedral aluminous smectites "Sm" — BO6, 200 m. (b) Primary pyroxene pseudomorphosed by chlorite "Ch", He: hematite — BO6, 160 m. (c) Strongly destructive illitization of the host rock as observed in the sealed part of the damage zone of the Plateau fault. Il: illitic material, Py: pyrite — BO6, 650 m. (d) Vug filled by chlorite "Ch"+fibrous epidote "Ep" — BO6, 836 m.

characteristic of boiling zones (Tulloch, 1982; Simmons and Christenson, 1994), have been locally observed.

5.2. The illite zone

This zone, located between 300 and 700 m depth ($180 < T < 250$ °C), is characterized by a secondary mineral assemblage consisting of illite ±illite-rich I–S mixed-layers±chlorite+quartz with lesser amounts of calcite, pyrite and/or hematite (Fig. 5c). This alteration pattern is particularly well expressed just below the first productive level (*i.e.*, between 600 and 660 m depth) where it is related to a strong destruction of the rock structure. Features of syn-crystallization of illite and chlorite (±pyrite) have been identified at these levels, suggesting the occurrence of at least two generations of chlorite. Quartz with pseudo-acicular texture (according to Dong et al., 1995) are identified around 350 m.

Out of the strongly illitized levels, evidence of earlier pervasive alteration features is underlined by pseudomorphous replacement of primary minerals and vug fillings by disseminated epidote+quartz+chlorite±corrensite±wairakite±prehnite±calcite±hematite. Corrensite was identified in weakly altered massive lava flows at 300–310 m ($T \approx 180$ °C) and 415 m ($T \approx 200$ °C) (Fig. 4).

5.3. The chlorite zone

The pervasive alteration predominates between 700 and 900 m depth (250–260 °C) out of the upper fractured zone of the Plateau fault and its related alteration haloes. The pervasively altered rocks are composed of chlorite+epidote+quartz (±calcite±hematite) (Fig. 5d). Illitization is still perceptible but the general trend is a decrease of illite amounts with increasing drilled depth. So, chlorite largely predominates over illite in the deeper part of BO6 well (770 to 910 m).

6. Variation of crystal structure and chemistry of index clay minerals

6.1. Smectite

The dioctahedral character of the smectite is suggested by its (06,33) XRD reflection near 1.49 to 1.50 Å d-spacing (Fig. 3).

Their average structural formulas are given in Table 5. They were calculated from punctual analyses of smectites within plagioclases pseudomorphs, vein or vesicle infillings and clay matrix related to intensely altered areas. Analyses have been performed on selected microsites (to avoid contamination by kaolin or mixed layers minerals). The formulas are based on the following assumptions: a tetrahedral occupation fixed at 4 cations per $O_{10}(OH)_2$, Fe is arbitrary considered as Fe^{3+}, and no Mg was assigned in the interlayer sites.

All the smectites are dioctahedral and contain Al-rich octahedral layers. Their octahedral cationic occupancy varies between 1.98 and 2.02 and their layer charge, mostly compensated by Ca hydrated cations, ranges between 0.41 and 0.52 per $O_{10}(OH)_2$. The percentage of the negative layer charge generated by tetrahedral substitution (Al for Si) varies from 60% to 85% and reaches 95–100% in samples collected respectively at 125 m (97 °C), 155 m (111 °C) and below 160 m (115 °C at 160 m and 130 °C at 185 m). Such a crystal chemical variation is typical of a downward increase of the beidellite end-member within the dioctahedral smectites. Nearly pure beidellite was analyzed from and below 160 m depth (Table 5).

Table 5
Chemical analyses of smectites performed on samples BO6 125 m, BO5 155 m, BO5 160 m and BO5 185 m

Samples	125 m			155 m			160 m			185 m		
n.a.	16			11			18			14		
	an. ave.		s.d.	an. ave.		s.d.	an. ave.		s.d.	an. ave.		s.d.
Si	3.74		*0.07*	3.65		*0.02*	3.49		*0.04*	3.57		*0.04*
Al^{IV}	0.26		*0.07*	0.35		*0.02*	0.51		*0.04*	0.43		*0.04*
Al^{VI}	1.65		*0.08*	1.89		*0.02*	1.87		*0.06*	1.91		*0.03*
Fe^{3+}	0.18		*0.08*	0.04		*0.01*	0.08		*0.02*	0.03		*0.01*
Mg	0.16		*0.03*	0.08		*0.02*	0.07		*0.02*	0.06		*0.01*
Ti	0.00		*0.00*	0.00		*0.00*	0.00		*0.00*	0.01		*0.01*
Mn	0.00		*0.00*	0.00		*0.00*	0.00		*0.00*	0.00		*0.00*
OCT	1.99			2.01			2.02			2.01		
Ca	0.16		*0.02*	0.17		*0.01*	0.16		*0.04*	0.18		*0.02*
Na	0.05		*0.02*	0.03		*0.01*	0.06		*0.04*	0.05		*0.02*
K	0.05		*0.01*	0.04		*0.01*	0.14		*0.02*	0.03		*0.01*
INTCH	0.42			0.41			0.52			0.44		
% ch. T.	60			85			98			95		

n.a.: number of analyses; an. ave.: analytical average; s.d.: standard deviation; OCT: octahedral occupancy; INTCH: interlayer charge; % ch. T.: percentage of tetrahedral charge.

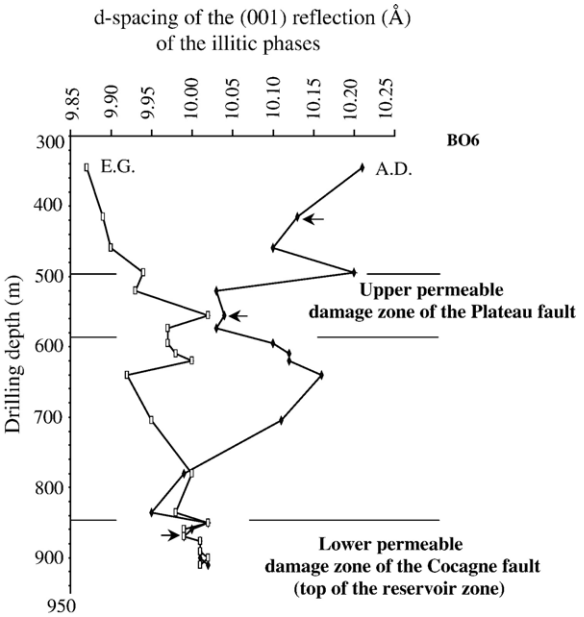

Fig. 6. d-spacing of the complex (001) reflection of the illitic phases (illite+illite-rich mixed-layers) in Å versus sample depth along BO6 well. A.D.: after air dry; E.G.: after ethylene–glycol saturation. Most of the samples consist of tuffs. The scarce lava samples are indicated by an arrow.

6.2. Illite

The XRD patterns of the illitic minerals from most of the investigated samples exhibit a complex peak near the (001) basal reflection of illite which is characteristic of a mixture of I–S mixed layer minerals with discrete illite. This mixture induces a typical change in both the peak profile and the position of the maximum intensity of the complex 10 Å reflection obtained after ethylene glycol solvation (Fig. 6). The deconvolution of such a complex 10 Å reflection (Fig. 7b) indicates that the expandable clay phases associated with discrete illite behave as ordered I–S mixed-layers ($R \geq 1$) with high illite content (higher than 85%). Ordered I–S mixed-layers ($R \geq 1$) with high illite content show a (001) peak with d-spacing between 10.5–12 Å that shifts and splits in two peaks after ethylene glycol solvation: a first one with d-spacing around 10.5–13 Å and a second one, more intense, with d-spacing around 9.5–10 Å. The lower the distance between the two aforementioned reflections obtained after ethylene glycol solvation, the higher the illite content of the

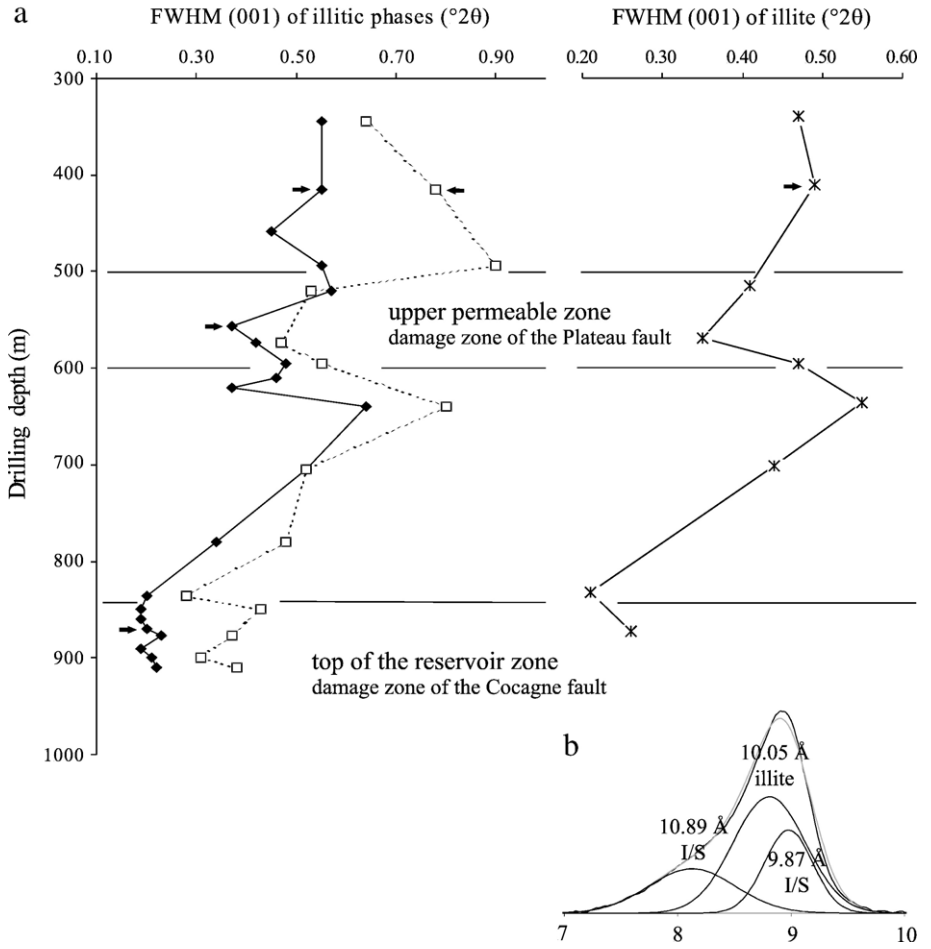

Fig. 7. (a) Full Width at Half Maximum intensity (FWHM) of the complex (001) reflection of the illitic material (°2θ, CuKα) versus sample depth along BO6 well. Black diamond: FWHM measured on the XRD of the <2 μm clay fraction; white square: FWHM measured on the XRD of the <0.2 μm clay fraction; crosses: FWHM of illite (001) basal reflection obtained after deconvolution of the XRD of the <0.2 μm fraction. (b) Example of deconvolution of the complex (001) reflection of the illitic material, I–S: ordered illite/smectite mixed-layers with high illite content. Most of the samples consist of tuffs. The scarce lava samples are indicated by an arrow.

ordered I–S mixed layers (Reynolds, 1980). It should be noted that the most perceptible effect of mixing illite rich ordered I–S mixed-layers with discrete illite on the peak profile of the complex 10 Å reflection consists of the shift of its maximum intensity toward lower position after ethylene glycol solvation (Fig. 6). This shift of the complex 10 Å reflection can be correlated with the global amount of expandable smectite layers in the illitic material, since the magnitude of the shift depends on both the respective amounts of illite and I–S mixed layers in the mixture, and the amount of expandable layers contained within the structure of the I–S mixed layer. Thus, the trend illustrated in Fig. 6 reveals an overall decrease of the amount of expandable smectite layers in the illitic material from 307 m to the accessible drilling depth (180 °C ≤ T ≤ 260 °C). However, the two permeable zones intersected between 520–574 m and 836–910 m deviate from the general trend since the illitic material is almost totally depleted in expandable layers, as illustrated by a nearly imperceptible shift of the 10 Å reflections, after the ethylene–glycol treatment: 0.02° 2θ (sample at 556 m) and <0.01° 2θ (from 850 m to the bottom), while I–S mixed layers are encountered on both sides of the upper permeable zone (around 500 and 620–640 m).

The FWHM values of the complex 10 Å reflection, measured on XRD patterns of <2 μm and <0.2 μm clay fractions, display an overall decrease with depth, apart from a local increase in

the range 550–620 m (Fig. 7a). The lower FWHM values correspond, as expected, to the illite-rich illitic material collected deeper than 836 m (0.19–0.22° 2θ) and between 550 and 620 m (0.42° 2θ). In order to clarify the evolution of the coherent scattering domain size of the pure illite, FWHM values were measured on the (001) reflection of illite obtained after deconvolution of the complex 10 Å reflection (Fig. 7a). The trend is similar to the aforementioned one, *i.e.*, a regular decrease with increasing depth (from 0.55 to 0.21° 2θ), except for the samples collected between 550 and 620 m.

Both morphologies and sizes of illite crystallites tend to change with increasing depth or temperature. Illite particles observed at shallow depth (345 m) are made of aggregates of thin crystallites with a fibrous morphology and an average width less than 1 μm (Fig. 8a). Deeper, the illite crystallites are coarser and they present two specific morphologies: (1) flaky shaped anhedral crystallites (average width: 1 to 3 μm) predominate within the clay matrices encountered at various depths (Fig. 8b); (2) subhedral to euhedral crystallites with hexagonal morphology and an average width of up to 10 μm predominate within the fractured horizons in which the geothermal fluids presently flow (Fig. 8c). The thickest hexagonal plates of illites have been observed at 574 m within the highly permeable damage zone of the Plateau fault (Fig. 8d).

Chemical analyses of illite±illite-rich I–S mixed-layers observed in altered plagioclases and vesicle

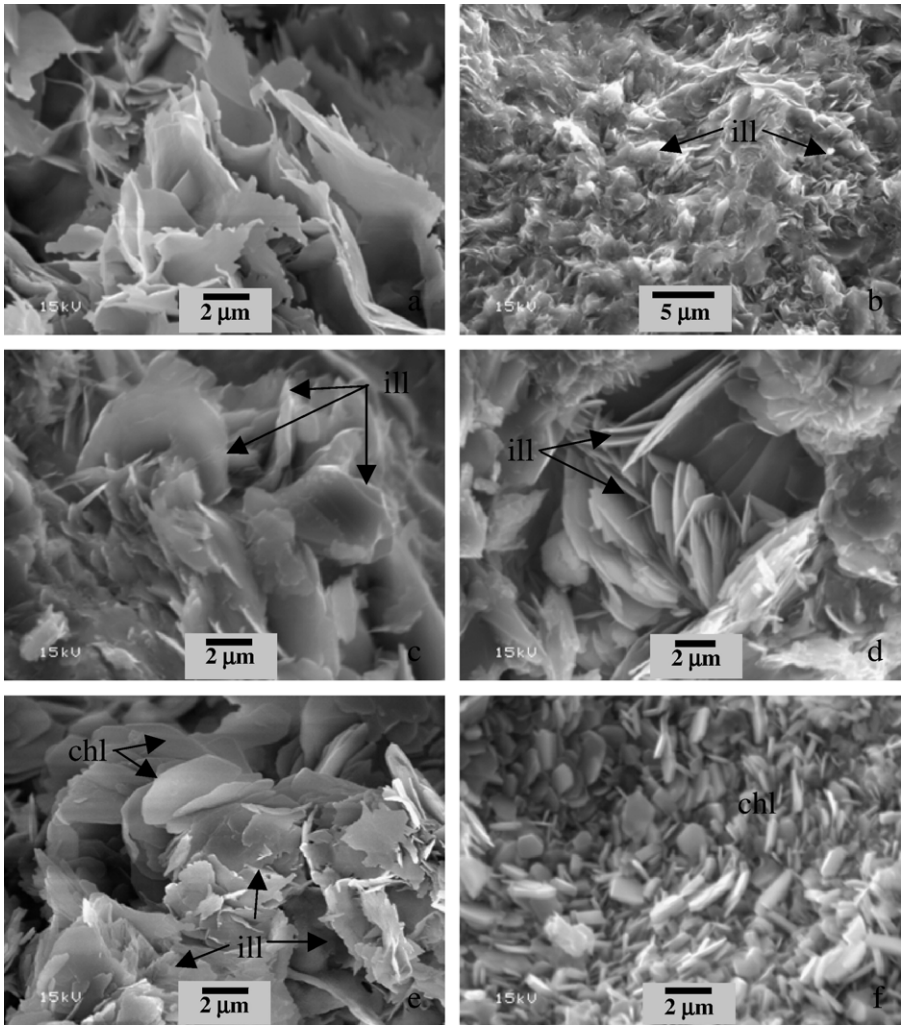

Fig. 8. Illitic phases and chlorite morphologies, SEM photographs in secondary electron mode. (a) BO6, 345 m; (b) BO6, 494 m; (c) BO6, 520 m; (d) BO6, 574 m. (e) BO6, 345 m; (f) BO6, 910 m. chl: chlorite; ill: illite+illite-rich mixed-layers. All the samples consist of tuffs.

Table 6
Chemical analyses of illite performed on samples BO6 415 m, 494 m, 520 m, 540 m, 595 m, 620 m, 640 m, 850 m and 910 m

Samples	415 m		494 m		520 m		540 m		595 m		620 m		640 m		650 m		850 m		910 m	
n.a.	6		16		9		7		33		19		9		94		9		8	
	an. ave.	s.d.	an. ave.	s.d.	an. ave.	s.d.	an. ave.	s.d.	an. ave.	s.d.	an. ave.	s.d.	an. ave.	s.d.	an. ave.	s.d.	an. ave.	s.d.	an. ave.	s.d.
Si	3.31	*0.04*	3.30	*0.04*	3.28	*0.06*	3.21	*0.04*	3.20	*0.05*	3.24	*0.05*	3.29	*0.02*	3.25	*0.06*	3.32	*0.03*	3.36	*0.05*
Al^{IV}	0.69	*0.04*	0.70	*0.04*	0.72	*0.06*	0.79	*0.04*	0.80	*0.05*	0.76	*0.05*	0.71	*0.02*	0.75	*0.06*	0.68	*0.03*	0.64	*0.05*
Al^{VI}	1.71	*0.02*	1.55	*0.05*	1.66	*0.06*	1.63	*0.06*	1.70	*0.07*	1.68	*0.05*	1.79	*0.02*	1.81	*0.04*	1.66	*0.03*	1.68	*0.02*
Fe^{3+}	0.14	*0.02*	0.25	*0.03*	0.17	*0.03*	0.24	*0.05*	0.17	*0.03*	0.20	*0.03*	0.10	*0.04*	0.11	*0.03*	0.17	*0.02*	0.12	*0.01*
Mg	0.10	*0.01*	0.18	*0.04*	0.17	*0.04*	0.13	*0.03*	0.14	*0.06*	0.13	*0.03*	0.07	*0.01*	0.08	*0.01*	0.14	*0.02*	0.15	*0.02*
Ti	0.00	*0.00*	0.00	*0.00*	0.00	*0.00*	0.00	*0.00*	0.00	*0.00*	0.00	*0.00*	0.00	*0.00*	0.00	*0.00*	0.00	*0.00*	0.00	*0.00*
Mn	0.01	*0.01*	0.01	*0.01*	0.01	*0.01*	0.01	*0.01*	0.00	*0.00*	0.01	*0.01*	0.01	*0.01*	0.01	*0.01*	0.00	*0.01*	0.01	*0.01*
OCT	1.97		1.99		2.01		2.02		2.01		2.02		1.99		2.01		1.97		1.96	
Ca	0.02	*0.07*	0.02	*0.01*	0.01	*0.01*	0.01	*0.00*	0.02	*0.02*	0.01	*0.01*	0.02	*0.02*	0.01	*0.02*	0.01	*0.01*	0.00	*0.00*
Na	0.06	*0.07*	0.02	*0.04*	0.03	*0.02*	0.01	*0.03*	0.05	*0.05*	0.05	*0.02*	0.03	*0.01*	0.04	*0.02*	0.02	*0.01*	0.02	*0.01*
K	0.79	*0.03*	0.84	*0.03*	0.78	*0.03*	0.82	*0.03*	0.80	*0.03*	0.79	*0.03*	0.74	*0.03*	0.74	*0.03*	0.87	*0.02*	0.85	*0.02*
INTCH	0.88		0.91		0.83		0.86		0.90		0.86		0.82		0.80		0.91		0.87	

n.a.: number of analyses; an. ave.: analytical average; s.d.: standard deviation; OCT: octahedral occupancy; INTCH: interlayer charge.

infillings are reported in Table 6. Their octahedral Al content ranges from 1.55 to 1.81 atoms per $O_{10}(OH)_2$ (average values) for an octahedral occupancy close to 2.00 (1.95–2.01). The average Fe and Mg contents range from 0.11 to 0.28 and from 0.06 to 0.18 at. per $O_{10}(OH)_2$, respectively. The interlayer charges vary between 0.67 (318 m) and 0.87 (860 m). The chemical effect of the very low amounts of expandable layers evidenced by XRD seems imperceptible (*i.e.*, there is no correlation between the amount of expandable layers determined from the XRD investigations and the interlayer charges calculated from the chemical microanalyses).

6.3. Chlorite

In order to minimize the influence of corrensite associated in places with chlorite, the FWHM of chlorite was measured on the (002) reflection instead of the (001) reflection. Both infra 2 μm and infra 0.2 μm fractions were studied, before and after ethylene–glycol treatment. In both clay fractions, the general trend is a decrease of the FWHM with increasing depth (Fig. 9), with the exception of the samples located around 640 m in which FWHM values measured on both <2 μm and <0.2 μm XRD patterns are much lower than those expected.

The textural properties of chlorite have only been determined for the crystallites formed in the porous media of the altered rocks (vugs, microfractures). The chlorite crystallites are euhedral and exhibit a subhexagonal shape with an average width ranging from 2 to 5 μm (Fig. 8e). Coarsening of euhedral chlorite proceeds essentially by thickening of crystals along the c* axis leading to blockier and more rigid plates at greater depth (Fig. 8f).

The chemical compositions of chlorites analyzed for different depths between 310 m and 910 m agree with those of trioctahedral chlorites (Table 7). The structural formula are calculated on the basis of 14 oxygens, assuming the total iron as Fe^{2+}. Octahedral Al is higher than tetrahedral Al. The octahedral layer occupancy is always lower than 6 (5.72 at.<oct. occ.<5.89 at.). The lower values (<5.8) are not systematically accompanied by interlayer charges that would be consistent with the presence of minor amounts of expandable phases (such as corrensite for instance).

If we except the samples collected around 620–640 m, the chlorite chemical variation is generally weak at the sample scale (Fig. 10). In the former samples, two populations of chlorite have been identified on the basis of their XFe ratio (Fe/(Fe+Mg)): (1) a pervasive chlorite observed as pseudomorph of ferromagnesian minerals which is relatively depleted in iron compared to (2) the iron-rich chlorite associated with illite (±pyrite) as vug infillings.

At the drill hole scale, the most significant chlorite compositional variation concerns the XFe ratio which ranges from 0.31 to 0.80. Two different chemical behaviors were determined. Both pervasive chlorites and bulk rock display a nearly parallel variation of XFe ratio through most of the intersected volcanic formations. Conversely, these XFe ratios vary in an inverse way in the two main permeable zones identified between

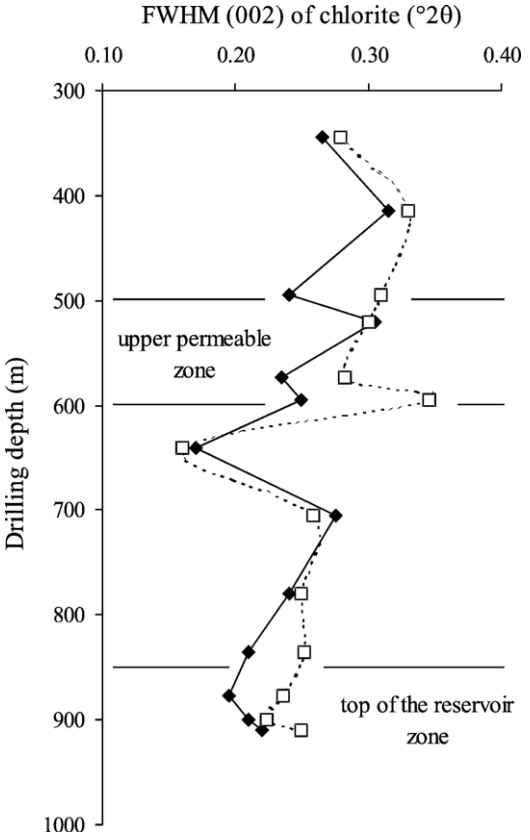

Fig. 9. Full Width at Half Maximum intensity of the (002) reflection of chlorite (°2θ, CuKα) versus sample depth along BO6 well. Black diamond: FWHM measured on the XRD of the <2 μm clay fraction; white square: FWHM measured on the XRD of the <0.2 μm clay fraction. All the samples consist of tuffs.

500 and 600 m and below 900 m depth, respectively (Fig. 11).

7. Discussion

7.1. The vertical distribution of clay minerals: a classical pattern

The vertical distribution of the clay minerals identified in BO6 drill hole is organized in three main zones: a 280-m-thick shallow alteration zone dominated by dioctahedral smectites, an intermediate alteration zone (between 280 and 700 m depth) dominated by illitic minerals and a deep alteration zone dominated by chlorite. However, the petrographic examinations demonstrated that this vertical distribution was not the result of a single hydrothermal event but rather the manifestation of at least two successive alteration stages during the thermal history of the Bouillante geothermal field.

The first alteration stage has been assimilated to the propylitic alteration extensively described in the literature (Lowell and Guilbert, 1970; Titley et al., 1986; Beaufort et al., 1990; Berger and Velde, 1992; Inoue, 1995, among others). Propylitic alteration is a widespread thermally controlled process which results from the interaction of nearly stagnant fluids of various origin (in pore and microcracks) with the most reactive primary mineral phases in rocks (pervasive alteration). The minerals attributed to the propylitic paragenesis consist mostly of trioctahedral phyllosilicates (chlorite or corrensite in weakly altered lavas), Ca-silicates (zeolites, prehnite, pumpelleyite, wairakite and epidote), quartz and minor calcite. According to the data on the thermal stability of these secondary phases (Inoue, 1995), the temperature probably reached 200 °C at depths shallower than 125 m during this first stage of alteration, suggesting a past geothermal gradient higher than nowadays.

The second stage of alteration is superimposed over the previously propylitized rocks and is characterized by a more or less intense argillization expressed by the occurrence of aluminous dioctahedral clay phases (smectite, scarce kaolinite and illite±I–S mixed layers) associated with quartz, calcite, hematite or pyrite. Several authors mentioned this type of alteration as argillic (for smectite rich assemblages and T<200 °C) or phyllic alteration (for non-expandable dioctahedral phases, and for 200 °C<T<300 °C) (Lowell and Guilbert, 1970; Beaufort et al., 1990; Pirajno, 1992). The occurrence of kaolinite, which is typical of advanced argillic alteration, may be related to fracture controlled limited circulations of more acid thermal waters in the past (Wohletz and Heiken, 1992). Such acid fluids could result from acid condensates located above underground boiling zones (Henley and Ellis, 1983).

In fluid dominant hydrothermal systems, these alterations are well known to have developed in zones of active flow regime structurally controlled by fracture networks. During this alteration stage, the temperatures were probably close to those presently measured in the wells, since saturation calculations performed using the EQ3NR geochemical code suggest that the aforementioned 2:1 clay minerals are in chemical equilibrium with the geothermal fluids at the measured downhole temperatures (Traineau et al., 1997; Sanjuan et al., 2001). All the above considerations suggest that the parageneses of the second stage of alteration constitute the signature of the recent to present circulation of geothermal fluids within the Bouillante geothermal field.

The vertical distribution of the dioctahedral clay minerals resulting from the geothermal activity of the

Table 7
Chemical analyses of some chloritic material

Samples	310 m		415 m		520 m		574 m		574 m		574 m		595 m		620 m	
an. loc.	Plagio		Plagio				Plagio		Vug		FeMg				Vug	
n.a.	8		5		11		10		10		8		14		12	
	an. ave.	s.d.	an. ave.	s.d.	an. ave.	s.d.	an. ave.	s.d.	an. ave.	s.d.	an. ave.	s.d.	an. ave.	s.d.	an. ave.	s.d.
Si	3.12	*0.04*	3.03	*0.10*	3.04	*0.07*	2.97	*0.05*	2.99	*0.05*	2.98	*0.04*	2.96	*0.06*	2.97	*0.05*
Al_{IV}	0.88	*0.04*	0.97	*0.10*	0.96	*0.07*	1.03	*0.05*	1.01	*0.05*	1.02	*0.04*	1.04	*0.06*	1.03	*0.03*
Al_{VI}	1.09	*0.02*	1.17	*0.13*	1.43	*0.06*	1.27	*0.04*	1.28	*0.04*	1.23	*0.03*	1.36	*0.06*	1.36	*0.06*
Ti	0.00	*0.00*	0.00	*0.00*	0.00	*0.00*	0.01	*0.00*	0.00	*0.00*	0.00	*0.00*	0.00	*0.00*	0.00	*0.00*
Fe^{2+}	1.79	*0.06*	2.39	*0.12*	1.42	*0.07*	1.96	*0.05*	2.06	*0.07*	2.12	*0.06*	1.34	*0.10*	2.36	*0.24*
Mn^{2+}	0.09	*0.01*	0.04	*0.01*	0.09	*0.02*	0.07	*0.01*	0.09	*0.02*	0.09	*0.01*	0.11	*0.03*	0.08	*0.02*
Mg^{2+}	2.86	*0.08*	2.26	*0.13*	2.78	*0.06*	2.52	*0.07*	2.39	*0.06*	2.41	*0.06*	2.99	*0.12*	1.98	*0.24*
OCT	5.83		5.86		5.72		5.83		5.82		5.85		5.80		5.78	
Ca	0.04	*0.01*	0.04	*0.01*	0.01	*0.01*	0.03	*0.00*	0.03	*0.01*	0.03	*0.01*	0.01	*0.00*	0.01	*0.00*
Na	0.01	*0.00*	0.00	*0.01*	0.03	*0.01*	0.01	*0.01*	0.02	*0.01*	0.01	*0.01*	0.02	*0.01*	0.05	*0.02*
K	0.00	*0.00*	0.00	*0.00*	0.01	*0.00*	0.00	*0.00*	0.00	*0.00*	0.00	*0.00*	0.02	*0.01*	0.02	*0.02*
INTCH	0.10		0.07		0.07		0.07		0.08		0.08		0.06		0.09	
Fe/(Fe+Mg)	0.38	*0.01*	0.52	*0.01*	0.34	*0.01*	0.44	*0.01*	0.46	*0.01*	0.47	*0.01*	0.31	*0.02*	0.54	*0.05*

Samples	620 m		640 m		640 m		705 m		836 m		860 m		860 m		910 m	
an. loc.	FeMg		FeMg		Vug		Vug				FeMg		Vug		FeMg	
n.a.	11		16		5		16		16		6		7		5	
	an. ave.	s.d.	an. ave.	s.d.	an. ave.	s.d.	an. ave.	s.d.	an. ave.	s.d.	an. ave.	s.d.	an. ave.	s.d.	an. ave.	s.d.
Si	3.05	*0.03*	2.83	*0.04*	2.75	*0.03*	3.02	*0.04*	2.86	*0.04*	3.03	*0.07*	2.92	*0.04*	2.88	*0.07*
Al_{IV}	0.95	*0.03*	1.17	*0.04*	1.25	*0.03*	0.98	*0.04*	1.14	*0.04*	0.97	*0.07*	1.08	*0.04*	1.12	*0.07*
Al_{VI}	1.41	*0.06*	1.45	*0.04*	1.62	*0.04*	1.34	*0.06*	1.29	*0.05*	1.23	*0.08*	1.37	*0.09*	1.38	*0.08*
Ti	0.00	*0.00*	0.01	*0.00*	0.01	*0.00*	0.00	*0.00*	0.00	*0.01*	0.00	*0.00*	0.00	*0.00*	0.01	*0.01*
Fe^{2+}	1.70	*0.08*	2.72	*0.07*	3.04	*0.09*	1.91	*0.08*	2.55	*0.05*	2.41	*0.08*	2.40	*0.10*	2.31	*0.07*
Mn^{2+}	0.07	*0.00*	0.12	*0.01*	0.35	*0.03*	0.05	*0.01*	0.10	*0.01*	0.07	*0.02*	0.08	*0.02*	0.16	*0.02*
Mg^{2+}	2.55	*0.06*	1.51	*0.06*	0.74	*0.02*	2.48	*0.08*	1.95	*0.03*	2.14	*0.03*	1.98	*0.09*	1.98	*0.06*
OCT	5.73		5.81		5.76		5.78		5.89		5.85		5.83		5.84	
Ca	0.02	*0.00*	0.02	*0.01*	0.01	*0.00*	0.02	*0.01*	0.02	*0.01*	0.01	*0.01*	0.01	*0.01*	0.01	*0.00*
Na	0.02	*0.01*	0.03	*0.01*	0.02	*0.01*	0.02	*0.01*	0.04	*0.03*	0.01	*0.01*	0.02	*0.02*	0.03	*0.02*
K	0.01	*0.01*	0.02	*0.01*	0.06	*0.03*	0.04	*0.02*	0.01	*0.01*	0.01	*0.01*	0.01	*0.01*	0.00	*0.00*
INTCH	0.07		0.09		0.11		0.09		0.09		0.04		0.05		0.05	
Fe/(Fe+Mg)	0.40	*0.01*	0.65	*0.01*	0.80	*0.01*	0.44	*0.01*	0.57	*0.01*	0.53	*0.01*	0.55	*0.01*	0.54	*0.01*

n.a.: number of analyses; an av: analytical average; s.d.: standard deviation; OCT: octahedral occupancy; INTCH: interlayer charge; an. loc.: microsite of crystallization; Fe–Mg: chlorite in replacement of ferromagnesian minerals; Vug: chlorite crystallized in vugs; Plagio: chlorite included in plagioclases (glass replacement).

Bouillante geothermal field is consistent with the "classical" distribution pattern established from many hydrothermal systems (Flexser, 1991; Inoue et al., 1992, 1999; Simmons and Browne, 1998, among others). The paragenesis of the shallowest alteration zone consists mostly of smectite locally associated with minor amounts of regularly ordered illite/smectite mixed-layers (I–S $R=1$) and is consistent with a mineral reaction in presence of near neutral geothermal waters. The dioctahedral smectites have intermediate crystal–chemical properties between those of beidellite and montmorillonite from the surface area to 125 m depth ($T \approx 100$ °C). Deeper, they are close to the beidellite composition. Nearly pure beidellite was identified at depths higher than 160 m and temperatures higher than 115 °C. Occurrence of smectites with crystal–chemical properties between those of montmorillonite and beidellite at shallow depth and temperature and of beidellite at greater depth and higher temperature was already reported by Yang et al. (2001) in the Broadlands–Ohaaki geothermal system. Such a temperature dependence of the crystal–chemical nature of the dioctahedral smectite in hydrothermal conditions agrees with the results of the experimental works of Yamada et al. (1991) and Yamada and Nakazawa (1993), who demonstrate that beidellite is stable at a higher temperature than montmorillonite. It

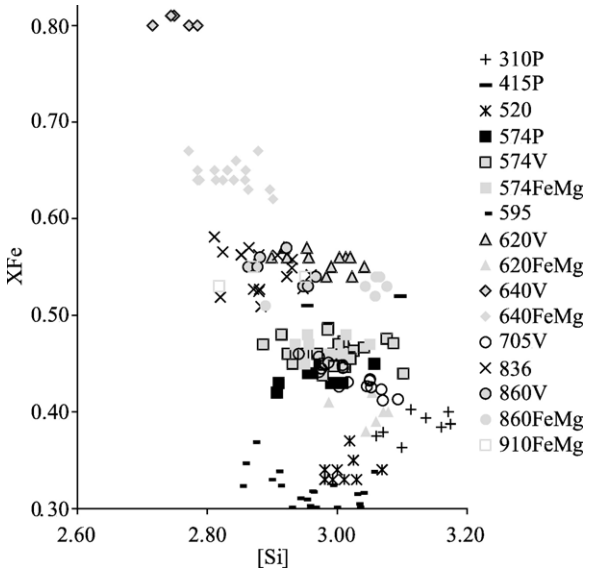

Fig. 10. Plot of some chlorite analyses in Fe/(Fe+Mg) (XFe) versus Si diagram for BO6 drill hole. V: chlorite crystallized in vugs, P: chlorite included in plagioclases (glass replacement) and FeMg: chlorite in replacement of pyroxenes. The size of the analyzed cuttings does not systematically allow to clarify the type of microsite of chlorite crystallization (no mention). Most of the samples consist of tuffs (excepted BO6-310 and 415).

also agrees with the observations of Beaufort et al. (1995) who identified beidellite as the characteristic smectitic component of high enthalpy geothermal reservoirs in which temperatures can exceed 200 °C.

Regularly ordered illite/smectite mixed-layers (I–S $R=1$) have been identified in association with the beidellitic smectites toward the bottom of the smectite zone (from 160 to 246 m).

Kaolinite is restricted to fractures which channeled more acid fluids at shallow depth (from 110 m to 230 m). It is linked to a fossil hydrothermal activity, associated with underground boiling, which occurred prior to the recent development of the smectites.

From 280 m to the bottom of the well, illitic minerals characterize both the intermediate and deep alteration zones in which fracture controlled permeable zones alternate with low permeable altered rocks.

7.2. The clay signature of the fracture controlled permeable zones

The permeable zones which channel most of the present geothermal fluids collected in well BO6 are fracture controlled and have been examined in more detail. Based on a preliminary petrographical examination, they do not exhibit any significant difference in clay mineralogy with their surrounding low permeable host rocks. Indeed, chlorite and illite+illite-rich mixed-layers are identified in zones of active flow regime as well as in zones of inactive flow regime. However, differences may be pointed out if we consider more specifically the crystal structure, the texture and/or the chemical properties of the clay minerals.

7.2.1. Signature of the illitic minerals

The broad transition of smectite to illite with increasing depth and temperature determined in the geothermal field of Bouillante is a general trend reported in both fossil and active hydrothermal systems (Bethke et al., 1986; Inoue et al., 1992; Yan et al., 2001) as well as in diagenetic environments (Sato et al., 1996; Dong et al., 1997). Such a transition has been considered as the result of a thermally activated sequential transformation reaction from smectite precursor to illite which proceeds via crystallization of I–S mixed layers series (Meunier and Velde, 1989) or as a result of simultaneous crystallization of all the I–S mixed layers via direct precipitation from solution (Inoue et al., 2004). In the geothermal field of Bouillante, the correlation between the decreasing amount of expandable layers within the illitic particles and the increasing temperature is not so clearly established. It seems effective over the whole zone of inactive flow regime but not at the

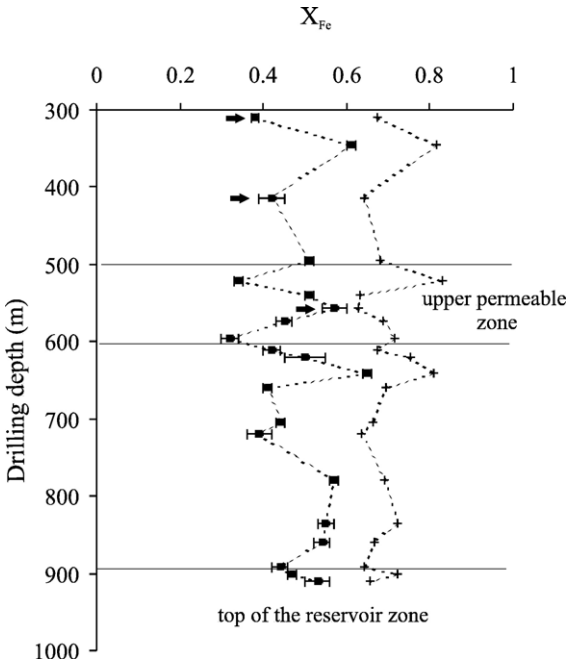

Fig. 11. Mean XFe values of both pervasive chlorite (black squares) and bulk rock (crosses) shown versus depth (BO6 drill hole). Most of the samples consist of tuffs. The scarce lava samples are indicated by an arrow.

level of the permeable zones which channel most of the present geothermal fluids (*i.e.*, the damage zones of the Cocagne and Plateau faults). Indeed, compared to those formed at similar temperatures within the surrounding low permeable altered rocks, the illitic minerals of the two main permeable zones (at 500–590 m and at 850–910 m) differ by a significant decrease in expandability associated with smaller FWHM values of the basal reflections (Figs. 6 and 7) and by the thickening of the subhedral to euhedral hexagonal crystallites (Fig. 8d). The cristallinity of the illitic material (along the c* axis and on the a,b plane) therefore appears enhanced in the levels which presently channel geothermal fluids.

In the present case, the intersected lithology is approximately homogeneous all along the drill hole, consisting mainly of hyaloclastic tuffs with very few intercalations of andesitic lava, and the chemistry of the geothermal fluids collected in the producing wells is very homogeneous. So, both the structural and textural variations of illitic minerals formed in the permeable fractured zones argue for a control of the rock permeability and the *F*/*R* ratio. These parameters are known to influence the kinetics of both the nucleation and the growth and transformation process of clay minerals (Inoue and Kitagawa, 1994). As a result, texture and crystal-structure of phyllosilicates are potential indicators of the circulation of fluids (past or present) in active geothermal systems (Flexser, 1991; Patrier et al., 1996; Teklemariam et al., 1996; Harvey and Browne, 2000; Mas et al., 2003). In high *F*/*R* ratio environment (*i.e.*, advective circulation of fluids in fractured host rocks) two scenarios may take place:

Ascending geothermal fluids become strongly oversaturated with respect to secondary clay material in response to abrupt changes in physical and chemical conditions (as a result of boiling or mixing of contrasting fluids for instance), and lead to explosive nucleation of clay crystallites with low size (Beaufort et al., 1996; Patrier et al., 1996).

Ascending fluids are weakly oversaturated with respect to clay minerals and lead to a much smaller nucleation rate, and in turn to a higher growth rate which leads to coarser (and more ordered) crystals of clay minerals (Inoue and Kitagawa, 1994).

In the first scenario, the mineral reactions take place far from chemical equilibrium and the nucleation of metastable phases is promoted. Such a crystallization process leads to the occurrence of heterogeneous mineral assemblages (for example, the different types of I–S mixed layers and illite which constitute the illitic minerals) as a result of a kinetically controlled conversion of the less stable phases to more stable ones according to the Ostwald step rule (Essene and Peacor, 1995; Altaner and Ylagan, 1997). We suggest that the strongly illitized level intersected by the drill hole BO6 at the bottom of the damage zone of the Plateau fault (around 640 m) occurred according to the above first scenario. The expected dramatic change of flow regime, related to the past tectonic activity of the fault, would have promoted temporary boiling of fluid (evidenced by the elongated crystal habits of secondary calcite and the occurrence of kaolinite at shallow depth) and crystallization of fine-grained illitic minerals containing higher amounts of expandable layers than in the surrounding samples. Similar observations have been noted in the Long Valley geothermal system by Flexser (1991) who interpreted the local occurrence of more expandable illitic minerals as the result of an earlier hydrothermal event that sealed the faulted zone and preserved it from more advanced illlization.

The second scenario seems to be presently operating in the fracture controlled permeable levels which channel the geothermal fluids in which it controls the crystallization of coarse grained subhedral platelets of nearly pure illite characterized by large CSD size.

7.2.2. Signature of chlorites

Since most of the chlorites were formed during the propylitic alteration stage (excepted in levels 620–640 m), their crystal-chemical and textural properties are much less informative on the fracture controlled permeable levels which presently channel the geothermal fluids. As a result, chlorites do not exhibit any specific variation of texture or crystal structure in the two zones of active flow regime intercepted by BO6. However, some geochemical differences have been noted concerning the partitioning of iron between chlorite and the other rock forming minerals in the shallower fractured zone which corresponds to the intersection of the Plateau fault. This is illustrated by the variation of XFe ratios in both the pervasive chlorites and the bulk rocks chemical analyses in BO6 drill hole (Fig. 11). With increasing depth, the XFe ratios of chlorites and bulk rock display a parallel variation in the non-productive zones, indicating that the chemistry of chlorite is rock dominated as specified by several authors in the altered rocks affected by the propylytic alteration (Shikazono and Kawahata, 1987; Beaufort et al., 1992; Lopez-Munguira et al., 2002). The XFe ratios of chlorites and their related bulk rock vary in an opposite way within the permeable zone identified close to the intersection of the Plateau fault, suggesting a fluid control there, as already reported in hydrothermal alteration of fractured rocks (Browne, 1989; Patrier et al., 1996). Changes of fO_2 of the hydrothermal fluid have frequently been invoked to

justify the aforementioned chemical behavior of chlorites (Nesbitt, 1990; Beaufort et al., 1992; De Caritat et al., 1993; Martinez-Serrano and Dubois, 1998). Indeed, the structural limitation in the assignment of Fe^{3+} in trioctahedral chlorite favours the incorporation of magnesium in the structure of chlorites which crystallize in association with hematite under oxidizing conditions (Beaufort et al., 1992). The specific crystal–chemical properties of the chlorites from the permeable zone related to the Plateau fault suggest that fluid circulation was effective during the propylitic alteration stage and consequently that the Plateau fault was already active at that time. The impossibility of collecting samples within the deeper fractured zone did not allow us to verify the past behavior of the Cocagne fault.

8. Concluding remarks

This study contributes to a better knowledge of the vertical distribution of alteration and the associated secondary clay minerals down to approximately 1000 m below the surface area of the geothermal field of Bouillante. It confirms that the geothermal fluids are presently channeled by the fracture networks associated with the Plateau and the Cocagne faults. Despite the andesitic average composition of the host rock, the fact that the youngest clay parageneses are mainly composed of dioctahedral clay minerals indicates that the spatial distribution of these clay minerals is essentially controlled by the chemistry of the infiltrating geothermal fluid and the temperature. In other words, these minerals precipitate from the ascending geothermal solutions and the general trend can be summarized by the vertical variation of the precipitated clay phases from illite to smectites (through various types of I–S mixed layers) with decreasing depth and temperature. However, the illitic phases which precipitated along the flow channels have specific structural and textural properties in response to the expected change of nucleation and growth rates operating in these high F/R ratio environments.

These new findings corroborate the previous work of Patrier et al. (2003) who proposed that the dioctahedral smectites which constitute the fracture filling material outcropping at several places in the area of Bouillante is a surficial indicator of the hidden high temperature geothermal system. The use of such a mineralogical tool could probably be valid for the prospection of hidden high temperature geothermal systems (*i.e.*, with few surface thermal manifestations), in geological settings similar to those of Bouillante (in West Indies and other oceanic subduction arc systems).

The absence of magnesian phases in the newly formed clay parageneses has to be related to the very low Mg content of the geothermal fluids extracted from the fracture networks associated with the Plateau and the Cocagne faults (less than 10 mg/l). As there is a major contribution of marine water to the geothermal fluids, as demonstrated by the previous geochemical studies (Sanjuan et al., 2001), it seems reasonable to expect that the geothermal fluids collected at Bouillante have precipitated significant amounts of magnesian clays in a deeper reservoir which still needs to be localized in more detail.

Further investigations on the oxygen and hydrogen isotopic composition would be necessary to improve our knowledge and our first interpretations on the relationship between clay properties and the present fluid circulation. However, these first conclusions are promising and underline the importance of studying clay minerals for geothermal prospection and evaluation of the future evolution of the Bouillante geothermal system.

Acknowledgments

Financial support for this study was provided by ADEME and the Research Division of BRGM. The authors are grateful to the staff of Geothermie Bouillante, CFG Services for site facilities.

References

Altaner, S.P., Ylagan, R.F., 1997. Comparison of structural models of mixed-layer illite/smectite and reaction mechanism of smectite illitization. Clays and Clay Minerals 45 (4), 517–533.

Beaufort, D., Westercamp, D., Legendre, O., Meunier, A., 1990. The fossil hydrothermal system of Saint Martin, Lesser Antilles: geology and lateral distribution of alterations. Journal of Volcanology and Geothermal Research 40, 219–243.

Beaufort, D., Patrier, P., Meunier, A., Ottaviani, M.M., 1992. Chemical variations in assemblages including epidote and/or chlorite in the fossil hydrothermal system of Saint Martin (Lesser Antilles). Journal of Volcanology and Geothermal Research 51, 95–114.

Beaufort, D., Papapanagiotou, P., Patrier, P., Traineau, H., 1995. Les interstratifiés I–S et C–S dans les champs géothermiques actifs: sont-ils comparables à ceux des séries diagénétiques? Bulletin des Centres de Recherches Exploration-Production Elf-Aquitaine 19, 267–291.

Beaufort, D., Papapanagiotou, P., Patrier, P., Fouillac, A.M., Traineau, H., 1996. I/S and C/S mixed layers, some indicators of recent physical–chemical changes in active geothermal systems: the case study of Chipilapa (El Salvador). Proceedings of the 21th Workshop on Geothermal Reservoir Engineering, Stanford, California.

Berger, G., Velde, B., 1992. Chemical parameters controlling the propylitic and argillic alteration process. European Journal of Mineralogy 4, 1477–1488.

Bethke, C.M., Vergo, N., Altaner, S.P., 1986. Pathways of smectite illitization. Clays and Clay Minerals 34, 125–135.

Brindley, G.W., Brown, G. (Eds.), 1980. Crystal structures of clay minerals and their X-ray identification. Mineral. Soc. London. 495 pp.

Brombach, T., Marini, L., Hunziker, J.C., 2000. Geochemistry of the thermal springs and fumaroles of Basse-Terre Island, Guadeloupe, Lesser Antilles. Bulletin of Volcanology 61, 477–490.

Browne, P.R.L., 1989. Contrasting alteration styles of andesitic and rhyolitic rocks in geothermal fields of the Taupo Volcanic Zone. In: Browne, P.R.L., Nicholson, K. (Eds.), Proceedings of the 11th New Zealand Geothermal Workshop. University of Auckland, pp. 111–116.

Cathelineau, M., Nieva, D., 1985. A chlorite solid solution geothermometer. The Los Azufres (Mexico) geothermal system. Contribution to Mineralogy and Petrology 91, 235–244.

Chrisditis, G.E., 1995. Mechanism of illitization of bentonites in the geothermal field of Milos Island, Greece: evidence based on mineralogy, chemistry, particle thickness and morphology. Clays and Clay Minerals 43, 569–585.

Correia, H., Sigurdsson, O., Sanjuan, B., Tulinius, H., Lasne, E., 2000. Stimulation of a high-enthalpy geothermal well by cold water injection. Geothermal Resources Council Transactions, vol. 24, pp. 129–136. September 24–27.

De Caritat, P., Hutcheon, I., Walshe, J.L., 1993. Chlorite geothermometry: a review. Clays and Clay Minerals 41 (2), 219–239.

Dong, G., Morrison, G., Jaireth, S., 1995. Quartz textures in epithermal veins, Queensland — classification, origin, and implications. Economic Geology 90, 1841–1856.

Dong, H., Peacor, D.R., Freed, R.L., 1997. Phase relations among smectite, $R=1$ illite–smectite, and illite. American Mineralogist 82, 379–391.

Drits, V.A., Srodon, J., Eberl, D.D., 1997. XRD measurements of mean crystallite thickness of illite and illite/smectite: reappraisal of the Kübler index and the Scherrer equation. Clays and Clay Minerals 45, 461–475.

Essene, E.J., Peacor, D.R., 1995. Clay mineral thermometry. A critical perspective. Clays and Clay Minerals 43 (5), 540–553.

Feuillet, N., Manighetti, I., Taponnier, P., Jacques, E., 2002. Arc parallel extension and localization of volcanic complexes in Guadeloupe, Lesser Antilles. Journal of Geophysical Research 107, B12 (2), 1–28.

Flexser, S., 1991. Hydrothermal alteration and past and present thermal regimes in the western moat of Long Valley caldera. Journal of Volcanology and Geothermal Research 48, 303–318.

Guggenheim, S., Bain, D.C., Bergaya, F., Brigatti, M.F., Drits, V.A., Eberl, D.D., Formoso, M.L.L., Galàn, E., Merriman, R.J., Peacor, D.R., Stanjek, H., Watanabe, T., 2002. Report of the Association Internationale pour l'Etude des Argiles (AIPEA) Nomenclature Comitee for 2001: order disorder and crystallinity in phyllosilicates and the use of the "Crystallinity Index". Clay Minerals 37, 389–393.

Harvey, C.C., Browne, P.R.L., 1991. Mixed-layer clay geothermometry in the Wairakei geothermal field, New Zealand. Clays and Clay Minerals 39 (6), 614–621.

Harvey, C.C., Browne, P.R.L., 2000. Mixed-layer clays in geothermal systems and their effectiveness as mineral geothermometers. Proceedings of the World Geothermal congress, Kyushu, Japan, May–June 10, 2000, pp. 1201–1205.

Henley, R.W., Ellis, A.J., 1983. Geothermal systems ancient and modern: a geochemical review. Earth Science Reviews 19, 1–50.

Horton, D.G., 1985. Mixed-layer illite/smectite as a paleotemperature indicator in the Amethyst vein system, Creede district, Colorado, USA. Contribution to Mineralogy and Petrology 91, 171–179.

Inoue, A., 1995. Formation of clay minerals in hydrothermal environments. In: Velde, B. (Ed.), Origin and Mineralogy of Clays. Springer, pp. 268–329.

Inoue, A., Kitagawa, R., 1994. Morphological characteristics of illite clay minerals from a hydrothermal system. American Mineralogist 79, 700–711.

Inoue, A., Utada, M., 1983. Further investigations of a conversion series of dioctahedral mica/smectite in the Shinzan hydrothermal alteration area, northeast Japan. Clays and Clay Minerals 31 (6), 401–412.

Inoue, A., Utada, M., Wakita, K., 1992. Smectite to illite conversion in natural hydrothermal systems. Applied Clay Science 7, 131–145.

Inoue, A., Utada, M., Shimizu, M., 1999. Mineral–fluid interactions in the Sumikawa geothermal system, northeast Japan. Resource Geology Special Issue 20, 79–98.

Inoue, A., Meunier, A., Beaufort, D., 2004. Illite–smectite mixed layer minerals in felsic volcaniclastic rocks from drill cores, Kakkonda, Japan. Clays and Clay Minerals 52, 66–84.

Jennings, S., Thompson, G.R., 1986. Diagenesis of Plio-Pleistocene sediments of the Colorado River delta, Southern California. Journal of Sedimentary Petrology 56, 89–98.

Ji, J., Browne, P.R.L., 2000. Relationship between illite crystallinity and temperature in active geothermal systems of New Zealand. Clays and Clay Minerals 48, 139–144.

Jowett, E.C., 1991. Fitting iron and magnesium into the hydrothermal chlorite geothermometer. GAC/MAC/SEG Joint Annual Meeting, Toronto, Program with Abstracts, p. 16. A62.

Kranidiotis, P., MacLean, W.H., 1987. Systematics of chlorite alteration at the Phelps Dodge massive sulphide deposit, Matagami, Quebec. Economic Geology 82, 1898–1911.

Kubler, B., 1968. Evaluation quantitative du métamorphisme par la cristallinité de l'illite: Etat des progrès réalisés ces dernières années. Bulletin du Centre de Recherches de Pau-SNPA 2 (2), 385–397.

Lanson, B., Besson, G., 1992. Characterization of the end of smectite-to-illite transformation: decomposition of X-ray patterns. Clays and Clay Minerals 40, 40–52.

Lonker, S.W., Fitz Gerald, J.D., Hedenquist, J.W., Walshe, J.L., 1990. Mineral–fluid interactions in the Broadlands–Ohaaki geothermal system, New Zealand. American Journal of Science 290, 995–1068.

Lopez-Munguira, A., Nieto, F., Morata, D., 2002. Chlorite composition and geothermometry: a comparative HRTEM/AEM-EMPA-XRD study of Cambrian basic lavas from the Ossa Morena Zone, SW Spain. Clay Minerals 37, 267–281.

Lowell, J.D., Guilbert, J.M., 1970. Lateral and vertical alteration and mineralization zoning in porphyry ore deposits. Economic Geology 65, 373–408.

McDowell, S.D., Elders, W.A., 1980. Authigenic layer silicate minerals in borehole Elmore 1, Salton Sea geothermal field, California, USA. Contributions to Mineralogy and Petrology 74, 293–310.

Martinez-Serrano, R.G., Dubois, M., 1998. Chemical variations in chlorite at the Los Humeros geothermal system, Mexico. Clays and Clay Minerals 46, 615–628.

Mas, A., Patrier, P., Beaufort, D., Genter, A., 2003. Clay-mineral signatures of fossil and active hydrothermal circulations in the geothermal system of the Lamentin Plain, Martinique. Journal of Volcanology and Geothermal Research 124, 195–218.

Meunier, A., Velde, B., 1989. Solid solutions in I/S mixed-layer minerals and illite. American Mineralogist 74, 1106–1112.

Meunier, A., Lanson, B., Beaufort, D., 2000. Vermiculitization of smectite interfaces and illite layer growth as a possible dual model for illite–smectite illitization in diagenetic environment: a synthesis. Clay Minerals 35, 573–586.

Nesbitt, B.E., 1990. Fluid flow and chemical evolution in the genesis of hydrothermal ore deposits. In: Nesbitt, B.E. (Ed.), Short course on fluids in tectonically active regimes of the continental crust, pp. 261–292.

Patrier, P., Papapanagiotou, P., Beaufort, D., Traineau, H., Bril, H., Rojas, J., 1996. Role of permeability versus temperature in the distribution of the fine (<0.2 μm) clay fraction in the Chipilapa geothermal system (El Salvador). Journal of Volcanology and Geothermal Research 72, 101–120.

Patrier, P., Beaufort, D., Mas, A., Traineau, H., 2003. Surficial clay assemblage associated with the hydrothermal activity of Bouillante (Guadeloupe, FWI). Journal of Volcanology and Geothermal Research 126, 143–156.

Pirajno, F., 1992. Hydrothermal mineral deposits, principles and fundamental concepts for the exploration geologists. Springer Verlag Ed. 709 pp.

Reynolds, R.C., 1980. Interstratified clay minerals. In: Brindley, G.W., Brown, G. (Eds.), Crystal Structures of Clay Minerals And Their X-ray Identification, Mineral. Soc. London, pp. 249–304.

Reynolds, R.C., 1985. Description of program NEWMOD for the calculation of the one-dimensional X-ray diffraction patterns of mixed-layered clays. Dept Earth Sciences, Dartmouth College, Hanover, New Hampshire, 23 pp.

Roberson, H.E., Lahann, R.W., 1981. Smectite to illite conversion rates: effects of solution chemistry. Clays and Clay Minerals 29, 129–135.

Sanjuan, B., Brach, M., Lasne, E., 2001. Bouillante geothermal fluid: mixing and water/rock interaction processes at 250 °C. In: Cidu, R. (Ed.), Proceedings of the 10th International Symposium on Water/Rock Interactions (WRI 10), vol. 2. A.A. Balkema publishers, Villasimius (Italy), pp. 911–914. 10–15 July 2001.

Sato, T., Murakami, T., Watanabe, T., 1996. Change in layer charge of smectites and smectite layers in illite/smectite during diagenetic alteration. Clays and Clay Minerals 44, 460–469.

Shikazono, N., Kawahata, H., 1987. Compositional differences in chlorite from hydrothermally altered rocks and hydrothermal ore deposits. Canadian Mineralogist 25, 465–474.

Simmons, S.F., Browne, P.R.L., 1998. Illite, illite–smectite and smectite occurrences in the Broadlands–Ohaaki geothermal system and their implications for clay mineral geothermometry. In: Arehart, G.B., Hulston, J.R. (Eds.), Proceedings of Water Rock Interaction-9, Balkema Rotterdam, pp. 691–694.

Simmons, S.F., Christenson, B.W., 1994. Origins of calcite in a boiling geothermal system. American Journal of Science 294, 361–400.

Teklemariam, M., Battaglia, S., Gianelli, G., Ruggieri, G., 1996. Hydrothermal alteration in the Aluto–Langano geothermal field, Ethiopia. Geothermics 25 (6), 679–702.

Titley, S.R., Thompson, R.C., Haynes, F.M., Manske, S.L., Robinson, L.C., White, J.L., 1986. Evolution of the fractures and alteration in the Sierra–Esperanza hydothermal system, Pima Country, Arizona. Economic Geology 81, 343–370.

Traineau, H., Sanjuan, B., Beaufort, D., Brach, M., Castaing, C., Correia, H., Genter, A., Herbrich, B., 1997. The Bouillante geothermal field (F.W.I.) revisited: new data on the fractured geothermal reservoir in light of a future simulation experiment in a low productive well. Proceedings of the 22nd Workshop on Geothermal Reservoir Engineering, Stanford, 1997, pp. 97–103.

Tulloch, A.J., 1982. Mineralogical observation on carbonates scaling in geothermal wells at Kawerau and Broadlands. Proceedings of New Zealand Geothermal Workshop, 4th October 1982, Auckland, pp. 131–134.

Wohletz, K., Heiken, G., 1992. In: Sharp, D.H., Simmons, L.M. (Eds.), Volcanology and Geothermal Energy. University of California Press. 432 pp.

Yamada, H., Nakazawa, H., 1993. Isothermal treatments of regularly interstratified montmorillonite–beidellite at hydrothermal conditions. Clays and Clay Minerals 41, 726–730.

Yamada, H., Nakazawa, H., Yoshioka, K., Fujita, T., 1991. Smectites in the montmorillonite–beidellite series. Clay Minerals 26, 359–369.

Yan, Y., Tillick, D.A., Peacor, D.R., Simmons, S.F., 2001. Genesis of dioctahedral phyllosilicates during hydrothermal alteration of volcanic rocks. II. The Broadlands–Ohaaki hydrothermal system, New Zealand. Clays and Clay Minerals 49, 141–155.

Yang, K., Browne, P.R.L., Huntington, J.F., Walshe, J.L., 2001. Characterising the hydrothermal alteration of the Broadlands–Ohaaki geothermal system, New Zealand, using short-wave infrared spectroscopy. Journal of Volcanology and Geothermal Research 106, 53–65.